creative commons
COMMONS DEED

저작자표시-비영리-변경금지 2.0 대한민국

이용자는 아래의 조건을 따르는 경우에 한하여 자유롭게

- 이 저작물을 복제, 배포, 전송, 전시, 공연 및 방송할 수 있습니다.

다음과 같은 조건을 따라야 합니다:

저작자표시. 귀하는 원저작자를 표시하여야 합니다.

비영리. 귀하는 이 저작물을 영리 목적으로 이용할 수 없습니다.

변경금지. 귀하는 이 저작물을 개작, 변형 또는 가공할 수 없습니다.

- 귀하는, 이 저작물의 재이용이나 배포의 경우, 이 저작물에 적용된 이용허락조건을 명확하게 나타내어야 합니다.
- 저작권자로부터 별도의 허가를 받으면 이러한 조건들은 적용되지 않습니다.

저작권법에 따른 이용자의 권리는 위의 내용에 의하여 영향을 받지 않습니다.

이것은 이용허락규약(Legal Code)을 이해하기 쉽게 요약한 것입니다.

Disclaimer

dCollection

공학석사 학위논문

Acceleration of S_N Eigenvalue Calculation with Coarse Mesh Formulation Employing Angular Flux Discontinuity Factors

각불연속인자가 적용된 소격격자모델을 이용한 S_N 고유치 계산의 가속

2014년 8월

서울대학교 대학원

에너지시스템 공학부

임 채 호

Abstract

A homogenized coarse mesh S_N formulation employing angular flux discontinuity factors (AnDFs) is derived as a means of efficient acceleration of the underlying two-dimensional heterogeneous fine mesh transport calculations. The homogenization parameters for the coarse mesh S_N problem are generated by using the partially converged fine mesh heterogeneous S_N solution and the solution of the homogenized coarse mesh S_N problem provides the fine mesh problem with fast converging global fission source distributions. In order to make the coarse mesh S_N problem equivalent with the reference heterogeneous problem, the angle dependent homogenized total cross sections as well as AnDFs are employed. While the angle dependent total cross sections are directly generated from the partially converged fine mesh problem solution, the AnDFs are generated by using the solution of the pilot coarse mesh calculation in which AnDFs are not used. In addition to spatial homogenization, angular condensation is employed in the coarse mesh problem for faster acceleration. It is confirmed by solving a few cases of severely heterogeneous problems that the homogenized problem can be made fully consistently with the reference heterogeneous problem with these homogenization parameters. It is observed that large errors of about 1400 pcm in reactivity and 7 % in the fission source distribution encountered in the

mere volume weighted homogenization case disappear with the use of AnDFs and the angle dependent total cross sections.

An alternating calculation scheme involving the fine mesh and coarse mesh S_N calculations is set up to accelerate the power iteration of the fine mesh calculation by adjusting the fine mesh fission source distribution using the coarse mesh one through the modulation process. It is demonstrated from the applications to various problems with different compositions and core sizes that the performance of the acceleration scheme is outstanding in that the number of the fine mesh S_N power iterations can be reduced below 10 while reproducing exactly the original solution regardless of the core size. In other words, it appears that the convergence of the coarse mesh S_N formulation does not reveal any significant dependence on the problem size so that the effectiveness of the acceleration scheme becomes stronger for the larger problems having higher dominance ratios leading to a significant reduction in the computing time by a factor 84 for a 9x9 fuel assembly quarter core test problem.

Keywords:

Discrete Ordinates Method

Coarse Mesh Formulation

Angular Flux Discontinuity Factors

Student Number: 2012-23284

Contents

List of Tables

List of Figures

Chapter 1. Introduction

1.1 Backgrounds

In general, a very fine structure is required for the application of a transport method to a reactor problem which involves severely varying flux distributions inside a fuel cell. Thus a tremendously large problem is formed to solve a reactor problem with the S_N method which is extremely difficult to solve without a massively parallel computer. If a homogenized mesh is used in the S_N calculation, however, the computational burden can be significantly reduced. The concern is then how to generate homogenization parameters for the coarse mesh S_N calculation which might be based on finer mesh heterogeneous solutions to construct the homogenized problem equivalent with the heterogeneous fine mesh S_N problem.

In the view of the generalized equivalence theory [1], a homogenized problem can be fully consistent with the heterogeneous problem by introducing additional degree of freedom such as the

discontinuity factors (DFs) or the current correction factors. If these adjustment factors are obtained properly from the higher order heterogeneous problem, the homogenized problem can reproduce exactly the same result as the original heterogeneous problem even though the homogenized problem employing much coarser meshes is much easier and faster to solve. Its solution can thus be used to accelerate the underlying heterogeneous solution. The typical example is the coarse mesh finite difference formulation (CMFD) [2] to accelerate the method of characteristic (MOC) solutions as employed in several MOC codes [3,4]. The equivalent formulations, however, have employed a diffusion equation like formulation even in the case of accelerating the transport solutions. The diffusion equation like equivalent formulation does not have any limitation or problem as long as the underlying transport problem is a three-dimensional (3-D) problem. However, it is very inefficient to solve a 3-D transport problem with subpin level details. A compromising idea is to solve planar (2-D) fine mesh transport problems to generate the

homogenized transport solution parameters and then solve the 3-D transport problem with the homogenized parameters. In this regard, the motivation for this work is to establish a scheme to formulate a coarse mesh transport S_N problem which is fully consistent with the underlying 2-D fine mesh transport problem. The approach to be used here is to employ angular flux discontinuity factors.

1.2 Objectives and Scopes

In order to accelerate the fine mesh heterogeneous solution, it is necessary to construct an equivalent homogenized problem to the heterogeneous fine mesh S_N problem. If the homogenization parameters are obtained properly from the reference heterogeneous problem, the homogenized problem can reproduce exactly the same result as the original heterogeneous problem.

In the construction of the homogenized problem, the flux volume weighting method is normally used to generate homogenized cross sections. If only the homogenized cross sections are used, however, the neutron net currents and reaction rates obtained from the

homogenized problem will not agree with those of the reference fine mesh heterogeneous solution. The root cause of the discrepancy is that the continuity conditions for both the surface flux and net current of the reference solution cannot be simultaneously satisfied in the homogeneous solution. To solve this problem, the continuity condition of the surface flux is discarded by the discontinuity factor in the homogenized problem. As the result, the net current at each surface and reaction rate are preserved.

In this work, proper homogenization parameters such as angular flux discontinuity factor and angle dependent homogenized total cross section are determined to make the coarse mesh S_N formulation consistent with the finer mesh S_N solution. The homogenization parameters are then employed to the one and two-dimensional discrete ordinates method to establish an equivalent coarse mesh S_N formulation. Finally, the acceleration scheme to solve an eigenvalue problem by power iteration with the S_N method employing the angular discontinuity factors is set up. To enhance the performance of the

acceleration scheme, an iteration control scheme is implemented. In addition, a scheme to condense the higher order S_N quadrature to the S_2 quadrature in the coarse mesh calculation is established in order to further reduce the computational burden of the homogeneous calculation.

1.3 Organization of Thesis

In Chapter 2 of this thesis, the multigroup discrete ordinates equation is derived from the Boltzmann transport equation and the finite difference method is applied to the multigroup discrete ordinates for finite differencing of the spatial variables. The transport solution scheme involving angular sweeping is then presented. In Chapter 3, the homogenization method is described in detail while and in Chapter 4 the angular discontinuity factors and angle dependent total cross sections are implemented to the multi-dimensional discrete ordinates equation. And using the equivalent coarse mesh S_N formulation, the acceleration scheme is set to accelerate the fine mesh heterogeneous solution. In Chapter 5, the consistency between the heterogeneous and

the homogenized problems is checked and performance of the AnDFs based S_N acceleration scheme is examined with regards to the convergence characteristics and computing time. Chapter 6 concludes the thesis.

Chapter 2. Discrete Ordinates Method

The discrete ordinates method is a simple and powerful method to solve the integro-differential Boltzmann transport equation. The key aspects of this method is that the solid angle is discretized into a number of segments and the neutron angular flux is represented within a segment with a representative value. The continuous angular variation is approximated using a finite set of discrete directions with corresponding directional weighting factors. The transport equation is solved for the discrete direction $\hat{\Omega}_m$, and integration over $\hat{\Omega}$ is replaced by a quadrature. In this work, the discrete ordinates method is used to solve the transport equation.

In following, the multigroup discrete ordinates equation is derived first from the Boltzmann transport equation. The finite difference method is then applied to the multigroup discrete ordinates equation for finite differencing of the spatial variables. At the end of this chapter, how to eliminate the negative flux by the subsequent

application of the difference method is given.

2.1 Multigroup Discrete Ordinates Equations

In the discrete ordinates method, the Boltzmann equation is solved for a number of discrete directions $\hat{\Omega}_m$, to each of which a weight w_m is associated. The weight is to represent the following integral for the scalar flux and current over the angle with a weighted summation as:

$$\phi(\vec{r},E)=\int_{4\pi}\varphi(\vec{r},\hat{\Omega},E)d\hat{\Omega}\cong\sum_m\omega_m\varphi_m(\vec{r},E) \tag{2.1}$$

$$\vec{J}(\vec{r},E)=\int_{4\pi}\hat{\Omega}\varphi(\vec{r},\hat{\Omega},E)d\hat{\Omega}\cong\sum_m\omega_m\hat{\Omega}_m\varphi_m(\vec{r},E) \tag{2.2}$$

where the weight is normalized such that

$$\sum_m w_m=1 \tag{2.3}$$

by defining the 4π multiplied discretized angular flux as:

$$\varphi_m(\vec{r},E)\equiv 4\pi\varphi(\vec{r},\hat{\Omega}_m,E)\,. \tag{2.4}$$

Apart from the factor 4π, this φ_m is the solution of the Boltzmann equation for the discrete directions $\hat{\Omega}_m$. The extraneous source will now be omitted and considerations restricted to isotropic scattering by using equation (2-5).

$$\Sigma_s(\vec{r}, E' \to E, \hat{\Omega}' \cdot \hat{\Omega}_m) \cong \frac{1}{4\pi} \Sigma_{s0}(\vec{r}, E' \to E). \tag{2.5}$$

The Boltzmann equation for an arbitrary direction $\hat{\Omega}_m$ becomes then:

$$\begin{aligned} &\hat{\Omega}_m \cdot \vec{\nabla} \varphi_m(\vec{r}, E) + \Sigma_m(\vec{r}, E) \varphi_m(\vec{r}, E) \\ &= \frac{\chi(\vec{r}, E)}{k} \int \nu \Sigma_f(\vec{r}, E') \phi(\vec{r}, E') dE' + S_m(\vec{r}, E) . \end{aligned} \tag{2.6}$$

The scattering source is simplified as:

$$\begin{aligned} S_m(\vec{r}, E) &= \int_0^\infty \int_{4\pi} \Sigma_s(\vec{r}, E' \to E, \hat{\Omega}' \cdot \hat{\Omega}_m) \tilde{\varphi}(\vec{r}, E', \hat{\Omega}') d\hat{\Omega}' dE' \\ &= \int_0^\infty \int_{4\pi} \frac{1}{4\pi} \Sigma_{s0}(\vec{r}, E' \to E) \cdot 4\pi \varphi(\vec{r}, E', \hat{\Omega}') d\hat{\Omega}' dE' \\ &= \int_0^\infty \Sigma_{s0}(\vec{r}, E' \to E) \phi(\vec{r}, E') dE' . \end{aligned} \tag{2.7}$$

The multigroup form is obtained by integrating Eq. (2.6) over the width of the g' th energy group, $\Delta E_{g'}$, and by replacing the integrals over the entire energy range by summations over all groups g'. In the

multigroup approximation, the above discrete ordinates equations are transformed into the following set of equations:

$$\phi_g(\vec{r}) \cong \sum_m \omega_m \varphi_{mg}(\vec{r}) . \tag{2.8}$$

$$\vec{J}_g(\vec{r}) \cong \sum_m \omega_m \hat{\Omega}_m \varphi_{mg}(\vec{r}) . \tag{2.9}$$

$$\hat{\Omega}_m \cdot \vec{\nabla} \varphi_{mg}(\vec{r}) + \Sigma_{mg}(\vec{r}) \varphi_{mg}(\vec{r}) = \frac{1}{k} \chi_g(\vec{r}) F(\vec{r}) + S_{mg}(\vec{r}) . \tag{2.10}$$

$$F(\vec{r}) = \sum_{g'} \nu\Sigma_{f,g'}(\vec{r}) \phi_{g'}(\vec{r}) . \tag{2.11}$$

$$S_{mg}(\vec{r}) = \sum_{g'} \Sigma_{s0,g' \to g}(\vec{r}) \phi_{g'}(\vec{r}) . \tag{2.12}$$

where the flux, current and fission spectrum are energy-integrated by denoting the integration over the energy group ΔE_g by $\int_g$ as:

$$\varphi_{mg} = \int_g \varphi_m dE, \ \phi_g = \int_g \phi dE, \ \vec{J}_g = \int_g \vec{J} dE, \ \chi_g = \int_g \chi dE . \tag{2.13}$$

The $\nu\Sigma_f$ and Σ_{s0} are flux-weighted as:

$$\nu\Sigma_{f,g} = \frac{\int_g \nu\Sigma_f(E')\phi(E')dE'}{\phi_g}. \tag{2.14}$$

$$\Sigma_{s0,g'\to g} = \frac{\int_{g'}\int_g \Sigma_{s0}(E'\to E)\phi(E')dE'dE}{\phi_{g'}}. \tag{2.15}$$

The total cross section is however weighted with the angular flux according to the Eq. (2.6), therefore it depends on angle $\hat{\Omega}_m$ as:

$$\Sigma_{mg} = \frac{\int_g \Sigma(E)\varphi_m(E)dE}{\varphi_{mg}}. \tag{2.16}$$

Since it would be preferable to have just the angle independent total cross section on the LHS of Eq. (2.6), the term $\Sigma_g\varphi_{mg} - \Sigma_{mg}\varphi_{mg}$ is added to the both sides of the Eq. (2.6) with the scalar flux weighted total cross sections:

$$\Sigma_g = \frac{\int_g \Sigma(E)\phi(E)dE}{\phi_g}. \tag{2.17}$$

Then the LHS of the multigroup Boltzmann equation has the desired form, containing only $\Sigma_g\varphi_{mg}$. The RHS, on the other hand, has

become contaminated by the term $(\Sigma_g - \Sigma_{mg})\varphi_{mg}$. The elimination of this term is obtained by substituting for φ_{mg} its P_0 approximation $\varphi \cong \frac{1}{4\pi}\phi$. The solution of the S_N equation is now reduced to the solution of Eq. (2.10), with Σ_{mg} replaced by Σ_g and the P_0 contribution to the source.

2.2 Finite Difference Scheme

The finite difference method is then applied to the multigroup discrete ordinates equation for finite differencing of the spatial variables. Consider the following Boltzmann transport equation in group g with the group index g omitted and the sources term $Q_m(\vec{r})$ representing the fission and scattering sources:

$$\hat{\Omega}_m \cdot \vec{\nabla}\varphi_m(\vec{r}) + \Sigma_t(\vec{r})\varphi_m(\vec{r}) = Q_m(\vec{r}) . \qquad (2.18)$$

The angular variables are discretized by taking the sets of values (ξ_m, η_m) as the *x* and *y* directional components of the discrete angle $\hat{\Omega}_m$. The streaming term is then represented as:

$$\hat{\Omega}_m \cdot \vec{\nabla} \varphi_m(\vec{r}) = \xi_m \frac{\partial \varphi_m(\vec{r})}{\partial x} + \eta_m \frac{\partial \varphi_m(\vec{r})}{\partial y} . \qquad (2.19)$$

To yield the following discrete ordinates equations in rectangular geometry:

$$\xi_m \frac{\partial \varphi_m(\vec{r})}{\partial x} + \eta_m \frac{\partial \varphi_m(\vec{r})}{\partial y} + \Sigma_t(\vec{r}) \varphi_m(\vec{r}) = Q_m(\vec{r}) . \qquad (2.20)$$

Now let's define a rectangular mesh by points x_i on the x-axis and by lines through y_j and x_i parallel to the x and y-axes.

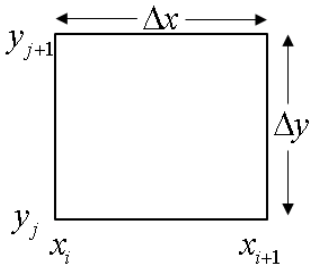

Fig. 2-1 2D Rectangular Mesh Area

The area bounded by x_i, x_{i+1} and y_j, y_{j+1} as shown in Fig. 2-1 is denoted by $\Delta V = \Delta x \Delta y = (x_{i+1} - x_i)(y_{j+1} - y_j)$ and it is assumed that all properties are constant inside ΔV.

To derive the difference relations for the rectangular mesh, integrate Eq. (2.20) over $x_i < x < x_{i+1}$ and $y_j < y < y_{j+1}$ for given direction $\hat{\Omega}_m$ as:

$$\xi_m \int_{y_j}^{y_{j+1}} \left(\varphi_m(x_{i+1}, y) - \varphi_m(x_i, y)\right) dy + \eta_m \int_{x_i}^{x_{i+1}} \left(\varphi_m(x, y_{j+1}) - \varphi_m(x, y_j)\right) dx + \Sigma_t \int_{y_j}^{y_{j+1}} \int_{x_i}^{x_{i+1}} \varphi_m(x, y) dx dy = \int_{y_j}^{y_{j+1}} \int_{x_i}^{x_{i+1}} Q_m dx dy. \tag{2.21}$$

Then define the fluxes averaged over the cell edges and area respectively as :

$$\varphi_{m,i+1} = \frac{1}{\Delta y} \int_{y_j}^{y_{j+1}} \varphi_m(x_{i+1}, y) dy \tag{2.22}$$

$$\varphi_{m,j+1} = \frac{1}{\Delta x} \int_{x_i}^{x_{i+1}} \varphi_m(x, y_{j+1}) dx \tag{2.23}$$

$$\varphi_m = \frac{1}{\Delta x \Delta y} \int_{y_j}^{y_{j+1}} \int_{x_i}^{x_{i+1}} \varphi_m(x, y) dx dy \tag{2.24}$$

and

$$Q_m = \frac{1}{\Delta x \Delta y} \int_{y_j}^{y_{j+1}} \int_{x_i}^{x_{i+1}} Q_m(x, y) dx dy . \tag{2.25}$$

The following equation is then obtained for ΔV.

$$\xi_m \Delta y(\varphi_{m,i+1} - \varphi_{m,i}) + \eta_m \Delta x(\varphi_{m,j+1} - \varphi_{m,j}) = V(Q_m - \Sigma_t \varphi_m). \quad (2.26)$$

The terms on the LHS represent the net losses caused by the x and y-components of the current in direction $\hat{\Omega}_m$, while the terms on the RHS are the gain form the source minus the losses from collision interactions. Eq. (2.26) contains no spatial approximations and therefore is exact.

Along with the expression of neutron balance, there are three unknowns with $\varphi_{m,i}$ and $\varphi_{m,j}$ known for the mesh area ΔV, but only one equation, Eq. (2.26). Two more equations are required to relate the cell average to the cell boundary fluxes. A relation frequently used is the weighted difference scheme which here, with $\xi_m > 0$ and $\eta_m > 0$, is given as:

$$\varphi_m = \omega \varphi_{m,i} + (1-\omega)\varphi_{m,i+1}. \quad (2.27)$$

$$\varphi_m = \omega \varphi_{m,j} + (1-\omega)\varphi_{m,j+1}. \quad (2.28)$$

With the weighting factor ω. If $\omega = 1$, it is the step difference scheme where φ_m is assumed constant across the mesh area except for the (i+1) and (j+1) boundaries. For $\omega = \frac{1}{2}$, it is the diamond difference scheme where φ_m is assumed to vary linearly between two opposite boundaries.

The manner in which these difference relationships are used depends on the incoming angle. The solution algorithm entails sweeping through the grid in the direction of neutron travel. As a result each iteration on the scattering source consists of four sweeps through the mesh :

$\xi_m > 0, \quad \eta_m > 0$ left to right; bottom to top. (1)

$\xi_m < 0, \quad \eta_m > 0$ right to left; bottom to top. (2)

$\xi_m > 0, \quad \eta_m < 0$ left to right; top to bottom. (3)

$\xi_m < 0, \quad \eta_m < 0$ right to left; top to bottom. (4)

For each case the weighted difference relationships are used as

follows :

$$\varphi_{m,i+1} = \frac{1}{1-\omega}(\varphi_m - \omega\varphi_{m,i}), \qquad \xi_m > 0 . \tag{2.29}$$

$$\varphi_{m,i} = \frac{1}{1-\omega}(\varphi_m - \omega\varphi_{m,i+1}), \qquad \xi_m < 0 . \tag{2.30}$$

$$\varphi_{m,j+1} = \frac{1}{1-\omega}(\varphi_m - \omega\varphi_{m,j}), \qquad \eta_m > 0 . \tag{2.31}$$

$$\varphi_{m,j} = \frac{1}{1-\omega}(\varphi_m - \omega\varphi_{m,j+1}), \qquad \eta_m < 0 . \tag{2.32}$$

When Eqs (2.29) and (2.32) are introduced into Eq. (2.26) to eliminate $\varphi_{m,i+1}$ and $\varphi_{m,j+1}$, this yields,

$$\varphi_m = \frac{Q_m V\bar{\omega} + \xi_m \Delta y \varphi_{m,i} + \eta_m \Delta x \varphi_{m,j}}{\xi_m \Delta y + \eta_m \Delta x + \bar{\omega} V \Sigma_t} . \tag{2.33}$$

where, $\bar{\omega}$ is $1-\omega$.

2.3 Negative Flux Fix-Up

It is obvious that Eq. (2.33) can't generate negative φ_m values as long as the boundary components $\varphi_{m,i}$ and $\varphi_{m,j}$ are positive. This is the physically correct and numerically desirable situation. The difference scheme may however produce the negative fluxes for

$\omega < 1$. It can be seen from Eq. (2.27) and (2.33) as:

$$\varphi_{m,i+1} = \frac{(\xi_m - \omega\Sigma_t\Delta x)\varphi_{m,i} + Q_m\Delta x}{\xi_m + \overline{\omega}\Sigma_t\Delta x}. \tag{2.34}$$

The above expression becomes negative if the numerator is negative. From this observation, $\varphi_{m,i+1}$ is positive when the following condition is satisfied.

$$(\xi_m - \omega\Sigma_t\Delta x)\varphi_{m,i} + Q_m\Delta x > 0. \tag{2.35}$$

Because it must be valid even for zero sources, the final condition is given as:

$$\Sigma_t\Delta x < \frac{\xi_m}{\omega}. \tag{2.36}$$

The negative angular fluxes can be generated if $\Sigma_t\Delta x$ is large. Further, it may occur for the small ξ_m values in high-order S_N approximations. Therefore, more fine meshes are needed to avoid the negative angular fluxes for various angles. In all cases, the risk is most pronounced when diamond differencing is used $(\omega = \frac{1}{2})$. This cannot

happen in the case of step differencing $(\omega = 1)$.

If the negative angular fluxes are generated, they can interrupt the iterative solution process. To avoid this, $\varphi_{m,i+1}$ is set to zero. At the same time, the newly calculated φ_m should be altered to preserve the neutron balance of Eq. (2.26). This is achieved by adding the negative term to the φ_m.

Although this scheme can eliminate the negative angular surface flux, it is not suitable for this work. To define the angular flux discontinuity factors, the homogeneous angular surface flux is needed and used as the denominator in the definition of the angular flux discontinuity factors. So, the angular surface flux shouldn't be set to zero. As the result, the step differencing is applied to the homogeneous problem to avoid the negative angular surface flux.

Chapter 3. Homogenization Method

Even with the rapid increase of computing power, direct treatment of detailed heterogeneous structure inside fuel assemblies is still prohibitive in the viewpoint of computation time and required memory storage. Current methods for reactor core calculations therefore involve a two-step approach in which lattice depletion transport methods are used to prepare energy collapsed and fuel assembly or pin cell homogenized cross section for subsequent whole core transport calculations [6]. Spatial homogenization requires both the actual boundary condition of the fuel assembly and the exact heterogeneous flux distribution of the whole core problem within that fuel assembly. Since the latter is not known a priori, an infinite medium condition is used in the lattice calculations. It is well known that this approximation may lead to undesirable errors in cores in which large flux gradients are present across the fuel assemblies. Therefore, reduction of spatial homogenization error is important for

accurate prediction of core characteristics, thus homogenization methods have been developed.

Various homogenization methods to mitigate spatial homogenization errors were proposed so far. One of the popular approaches is the generalized equivalence theory (GET). The GET is an extension of the discontinuity factor for neutron flux. One of the significant features of GET is derivation of homogenization parameters from single assembly calculations with reflective boundary condition. Since this condition is adopted in assembly calculations in actual in-core fuel management, no additional calculation is necessary to estimate the homogenization parameters for GET [9,10]. This feature simplifies the calculation preparing cross section set for core calculation codes and consequently contributes reduction of computation time.

The theory has many advantages as above but it cannot produce the reference heterogeneous solution perfectly. It is really important to eliminate homogenization error and make the homogenized problem

equivalent to the heterogeneous problem for accelerating the heterogeneous solution. To construct the homogenized problem fully consistent with the heterogeneous problem, an angle dependent homogenized cross section and newly defined angular discontinuity factor are employed to the homogenized problem in this work.

In following, the traditional flux-volume weighting method and generalized equivalence theory are reviewed as the foundation to construct the homogenized problem.

3.1 Flux-volume Weighting (FVW) Method

The FVW method is one of the traditional approaches for homogenization. In this method, the homogenized cross section is obtained as follows:

$$\bar{\Sigma}_{x,g}\bar{\phi}_g V = RR_{x,g}V = \bar{\Sigma}_{x,g}\sum_i^V \phi_{g,i}V_i = \sum_i^V \Sigma_{x,g,i}\phi_{g,i}V_i \tag{3.1}$$

$$\bar{\Sigma}_{x,g} = \frac{RR_{x,g}}{\bar{\phi}_g} = \frac{\sum_i^V \Sigma_{x,g,i}\phi_{g,i}V_i}{\sum_i^V \phi_{g,i}V_i} \tag{3.2}$$

$$\nu\bar{\Sigma}_{f,g} = \frac{\bar{\psi}_g}{\bar{\phi}_g} = \frac{\sum_i^V \nu\Sigma_{f,g,i}\phi_{g,i}V_i}{\sum_i^V \phi_{g,i}V_i} \tag{3.3}$$

$$\bar{\chi}_g = \frac{\sum_i^V \chi_{g,i}\bar{\psi}_i}{\bar{\psi}} = \frac{\sum_i^V \chi_{g,i}\sum_{g'}^G \nu\Sigma_{f,g',i}\phi_{g',i}V_i}{\sum_i^V \sum_{g'}^G \nu\Sigma_{f,g',i}\phi_{g',i}V_i} \tag{3.4}$$

where, $\bar{\Sigma}_{x,g}$ is the homogenized cross section for x reaction and $\Sigma_{x,g,i}$ is the cross section of region i. V_i is the volume of region i and $\phi_{g,i}$ is average flux of region i obtained by a heterogeneous calculation.

The most commonly employed procedures for determining homogenized parameters focus strictly on the preservation of reaction rates. If the volume-integrated neutron flux ($\sum_i^V \phi_{g,i}V_i$) obtained by the homogeneous calculation is identical with that of the heterogeneous calculation, the reaction rate in the reference calculation can be reproduced by the homogeneous calculation. However, if the homogenized cross section, which is derived from Eq. (3.1) through

(3-4), are directly used, the obtained neutron net currents among regions do not agree with those of the reference calculation. The use of conventional homogenized cross sections dose not directly addresses the issue of preservation of surface integrated currents and cannot be expected to preserve the properties of the heterogeneous problem. Consequently, reaction rates in the heterogeneous calculation cannot be reproduced by the FVW method. The fundamental cause of this discrepancy is the fact that continuity conditions both for the surface flux and the net current of the reference solution cannot be simultaneously satisfied in the homogenous calculation. To overcome this problem, advanced homogenization methods were issued. That will be described in the next section of this chapter.

3.2 Generalized Equivalence Theory (GET)

The persistence of large error in the solution to the homogenized problem even when exact flux-weighted cross sections are used indicates that the inaccurate approximation of the leakage terms is a major contributor to the error.

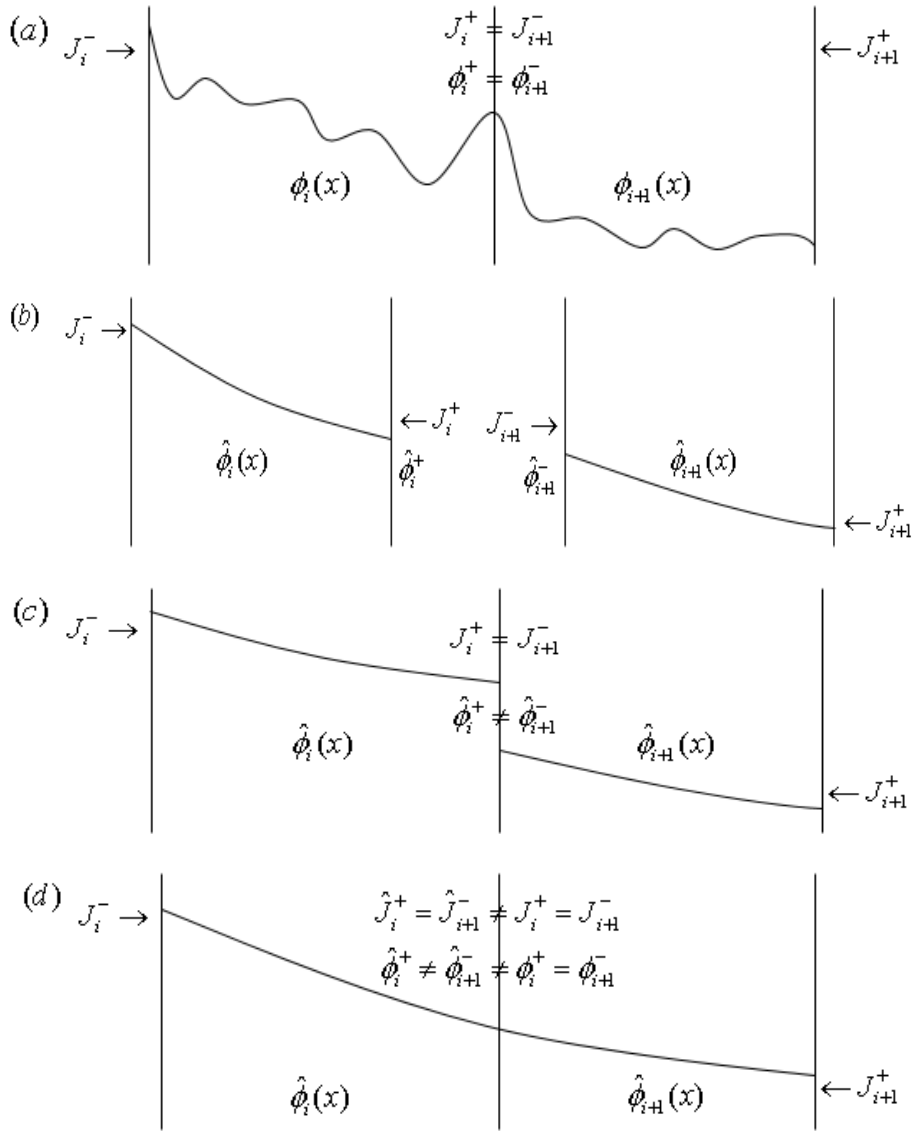

Fig. 3-1 One-dimensional Flux Distributions

(a) Heterogeneous problem flux
(b) Individual homogenized cells
(c) Adjacent individual homogenized cells
(d) Conventional homogeneous solution

Fig. 3-1 shows One-dimensional flux distributions. Herein, $\phi_i(x)$ is a heterogeneous average flux of homogenized cell i and $\hat{\phi}_i(x)$ is a homogenized average flux of the cell i. J_i is a surface current of the heterogeneous problem.

Then the difficulty of determining the appropriate values for the leakage term is described by considering a hypothetical one-dimensional problem. Let's consider two adjacent cells as depicted in Fig. 3-1(a). Exact flux-weighted cross sections can be computed, since the flux distribution is assumed to be known. Assuming that the known heterogeneous surface currents are imposed on the two surfaces of the cell i, the homogenized problem is fully specified. To make the surface currents be preserved for both of these cells, there exist one flux distribution which will satisfy the homogenized problem as depicted in Fig. 3-1(b).

Since the homogeneous flux distribution in each cell is directly affected by the value of the surface currents, the interface fluxes will be different as depicted in Fig. 3-1(c). As a direct result of the

difference between interface fluxes, the homogeneous flux distributions in both cell i and $i+1$ will be different than those of Fig. 3-1(c) when the homogenized problem for the two cells is solved with boundary conditions J_i^- and J_{i+1}^+, and continuity of flux and current interface conditions. An inevitable result of the different flux distributions in Fig. 3-1(d) shows that the homogeneous fluxes at the interface of cell isn't equal to the heterogeneous flux and also the homogeneous currents isn't equal to the heterogeneous interface current. Consequently, it is clear that the homogenized problem with the continuity condition for flux and current across interfaces lacks sufficient degrees of freedom to allow simultaneous preservation of reaction rates and currents.

In the generalized equivalence theory, the continuity condition of surface flux is discarded in the homogeneous calculation. If the homogeneous fluxes are allowed to be discontinuous, such as that depicted in Fig. 3-1(c), the heterogeneous flux distribution can be preserved when the homogenized problem is solved. Now let's

consider the flux distribution of Fig. 3-2.

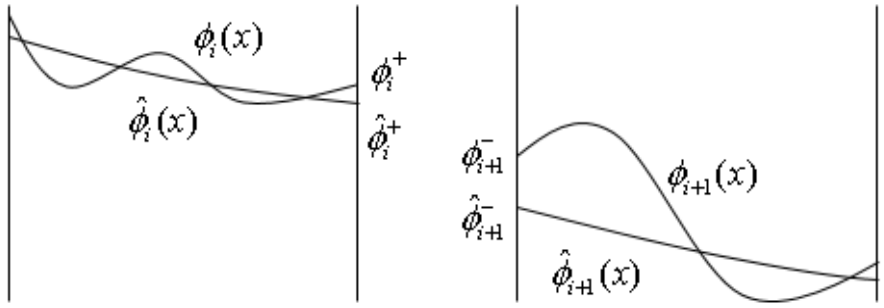

Fig. 3-2 One-dimensional Homogeneous Flux Distributions

The homogeneous flux distributions will be identical to those of Fig. 3-2 when the homogenized problem is solved, if an interface condition is imposed as:

$$\hat{\phi}_i^+ f_i^+ = \hat{\phi}_{i+1}^- f_{i+1}^- \tag{3.5}$$

where

$$f_i^+ \equiv \phi_i^+ / \hat{\phi}_i^+, \qquad f_{i+1}^- \equiv \phi_{i+1}^- / \hat{\phi}_{i+1}^- . \tag{3.6}$$

These f_i^+ and f_{i+1}^- are the discontinuity factor at right boundary of the cell i and discontinuity factor at left boundary of the cell $i+1$.

The Eq. (3.5) expresses that the heterogeneous flux is continuous across the interface and that there exists a direct relationship between the heterogeneous and homogeneous surface flux. When the homogenized problem is solved, the homogeneous flux is generated discontinuously by the discontinuity factors and the homogeneous flux distribution will be the same as that in Fig. 3-1(c), which results in the preservation of interface currents. The discontinuity factors can be considered to be additional homogenization parameters since they can be defined directly from information which is known from the reference solution. These discontinuity factors provide additional degrees of freedom which permit simultaneous preservation of reaction rates and surface currents.

Chapter 4. Angular Discontinuity Factors in Discrete Ordinates Equation

4.1 Angular Discontinuity Factors in Multi-dimensional Discrete Ordinates Equation

Before implementation of the angular discontinuity factors in two-dimensional discrete ordinates equation, the homogenization method is tested in one-dimensional equation for simplicity. After verification for effects of the angular discontinuity factors in 1-D, the homogenization method is applied to the 2-D discrete ordinates equation. Although implementation of the angular discontinuity factor is actually done for the weighted-difference flux evaluation method, the diamond differencing scheme is used to determine the angular average flux in the following for clarity.

4.1.1 Angular Discontinuity Factors in One-dimensional Discrete Ordinates Equation

The discretized Boltzmann transport equation for angle cosine μ_m is given as:

$$\mu_m \frac{d}{dx}\varphi_m + \Sigma_t \varphi_m = q_m . \tag{4.1}$$

Consider a homogenized cell (coarse mesh) i as depicted in Fig. 4-1. The homogenized coarse mesh cell is supposed to include many heterogeneous meshes inside.

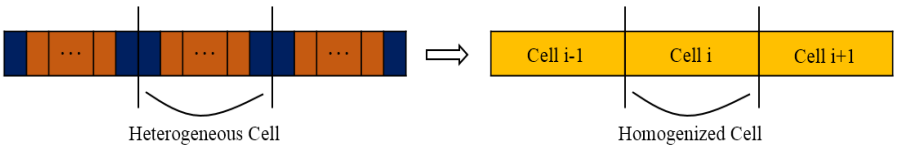

Fig. 4-1 Homogenized Cell i

The neutron balance equation for the cell i is obtained by integrating Eq. (4.1) over the cell i as:

$$\frac{\mu_m}{\Delta x_i}(\varphi_{i+1/2,m} - \varphi_{i-1/2,m}) + \bar{\Sigma}_t \varphi_m = q_m . \tag{4.2}$$

The homogenized cross section denoted by the overbar symbol is determined by the flux-volume weighting method.

In the view of the generalized equivalence theory, both volume integrated reaction rates and surface integrated currents of the

heterogeneous problem should be conserved in the homogenized problem. The current conservation can be achieved by introducing flux discontinuity at the cell interface. Particularly in transport calculation, this conservation can be met by approximating a linear shape of the angular flux within each homogenized cell and adjusting the degree of discontinuity at the interface. The discontinuous homogenized angular flux is shown in Fig. 4-2.

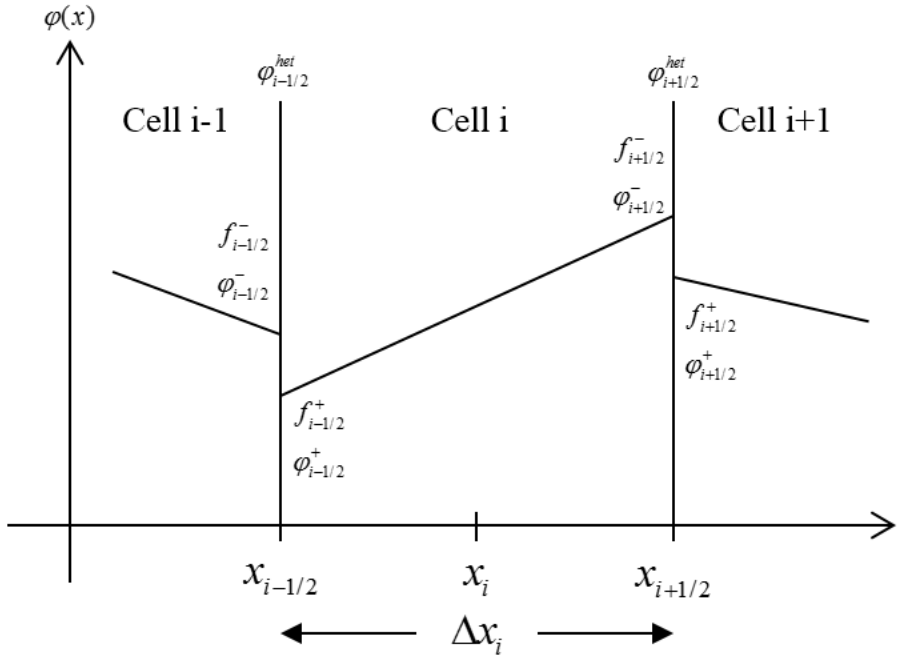

Fig. 4-2 Homogenized Angular Flux within Adjacent Computational Cells

The homogenized cell i is bounded by its left and right interfaces at $x_{i-1/2}$ and $x_{i+1/2}$ with adjacent cells $i-1$ and $i+1$. Each cell interface has two sides. The right hand side points toward larger x values and thus denoted by "$+$", and the other on the left by "$-$". By definition of the discontinuity factor, the flux continuity condition at $x_{i-1/2}$ is defined as [7,8]:

$$\varphi^{het}_{i-1/2,m} = f^{-}_{i-1/2,m}\varphi^{-}_{i-1/2,m} = f^{+}_{i-1/2,m}\varphi^{+}_{i-1/2,m} \tag{4.3}$$

where $f^{-}_{i-1/2,m}$ and $f^{+}_{i-1/2,m}$ are the angular discontinuity factors in each side of the interface. With the diamond difference relation, the cell average angular flux in cell i is expressed by the flux value at the midpoint of the cell as:

$$\varphi_m = \frac{1}{2}(\varphi^{+}_{i-1/2,m} + \varphi^{-}_{i+1/2,m}) = \frac{1}{2}(\frac{\varphi_{i-1/2,m}}{f^{+}_{i-1/2,m}} + \frac{\varphi_{i+1/2,m}}{f^{-}_{i+1/2,m}}) . \tag{4.4}$$

To make Eq. (4.1) for the homogenized cell i equal to the equation for the heterogeneous fine mesh, the homogeneous angular flux at each surface should be equal to the heterogeneous angular surface flux

and the homogeneous angular average flux should be equal to the heterogeneous angular average flux. This relation is shown as:

$$\frac{\mu_m}{\Delta x_i}(\varphi_{i+1/2,m}-\varphi_{i-1/2,m})+\bar{\Sigma}_t\varphi_m=q_m \rightarrow \frac{\mu_m}{\Delta x_i}(\varphi^{het}_{i+1/2,m}-\varphi^{het}_{i-1/2,m})+\bar{\Sigma}_t\varphi^{het}_m=q_m \ . \quad (4.5)$$

In the discrete ordinates method with finite differencing of the spatial variables, the neutron balance equation is calculated by the multiple spatial sweeps depending of angular directions.

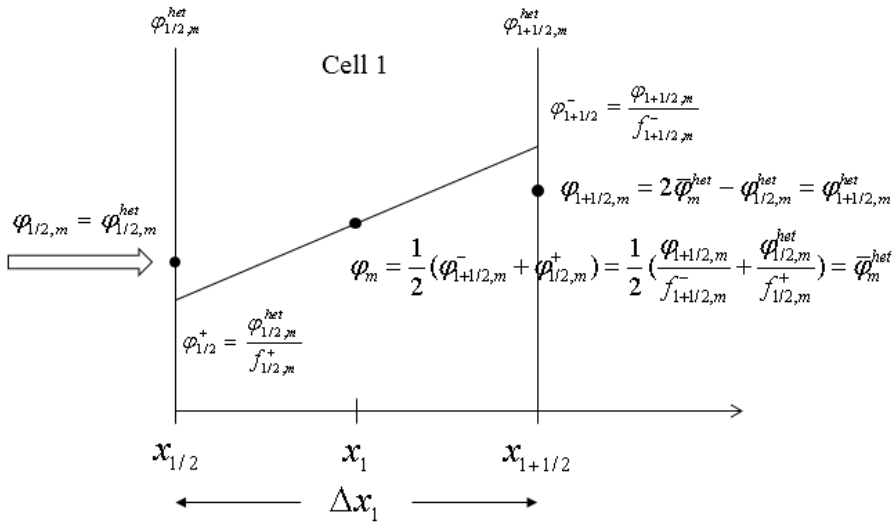

Fig. 4-3 Homogenized Angular Flux for First Cell

If the Eq. (4.5) is satisfied for the cell 1 (firstly calculated cell), the

relation should be satisfied for the overall space. Then, the homogenized coarse mesh formulation is equal to the heterogeneous fine mesh formulation. Firstly, the homogeneous angular surface flux at left surface of the cell 1 is equal to the heterogeneous surface flux by the boundary condition. Then, a discontinuous homogeneous angular flux is defined by the homogeneous angular surface flux and the discontinuity factor as shown in Fig. 4-3. To preserve the reaction rate at the cell 1, the homogenized cell average angular flux should be equal to the heterogeneous cell average angular flux. That condition is satisfied by the properly determined angular discontinuity factor. It will be treated in the next 4.1.2 section. Then, the right boundary angular flux can be defined by the left boundary angular flux and cell average angular flux. This process is depicted in Fig. 4-3. Finally, the homogeneous angular surface flux is equal to the heterogeneous angular surface flux and the homogeneous cell average angular flux is equal to the heterogeneous cell average angular flux. As the result, the homogenized coarse mesh formulation is equivalent to the

heterogeneous fine mesh formulation satisfying Eq. (4.5).

By using Eqs. (4.2) and (4.4), the homogenized cell average angular flux in cell i is obtained as:

$$\varphi_m = \left(2 f^-_{i+1/2,m} + \frac{\Sigma_t \Delta x_i}{\mu_m} \right)^{-1} \left(\left(1 + \frac{f^-_{i+1/2,m}}{f^+_{i-1/2,m}} \right) \varphi_{i-1/2,m} + \frac{\Delta x_i}{\mu_m} q_m \right). \quad (4.6)$$

In sweeping through spatial meshes toward the positive direction, Eq. (4.4) is used to obtain the right boundary angular flux of cell i.

$$\varphi^{het}_{i+1/2,m} = 2 f^-_{i+1/2,m} \varphi_m - \frac{f^-_{i+1/2,m}}{f^+_{i-1/2,m}} \varphi_{i-1/2,m} . \quad (4.7)$$

4.1.2 Determination of the Angular Discontinuity Factors

For the reaction rate conservation, the following identity should hold in the homogenized problem.

$$\varphi_m = \frac{1}{2} \left(\frac{\varphi^{het}_{i-1/2,m}}{f^+_{i-1/2,m}} + \frac{\varphi^{het}_{i+1/2,m}}{f^-_{i+1/2,m}} \right) = \bar{\varphi}^{het}_m . \quad (4.8)$$

The homogenized cell average angular flux should be equal to the heterogeneous cell average angular flux by using the angular discontinuity factors.

At first, The angular discontinuity factors are defined as the heterogeneous surface angular flux divided by the homogeneous surface angular flux in accordance with the GET. To generate the homogeneous surface angular flux, a pilot calculation for the homogenized problem constructed without imposing angular flux discontinuity is needed. Its solution is denoted by the superscript *hom* in the following.

The cell average angular fluxes of the homogenized problem with the above angular discontinuity factors are not the same as the reference cell average angular flux obtained for the heterogeneous problem. Fig. 4-4(a) shows the heterogeneous and homogeneous cell average angular flux for the cell i. When the angular discontinuity factors by the GET are used, the Eq. (4.8) is not hold and the reaction rate is not preserved in the homogenized problem. To make the homogenized cell average flux same with the heterogeneous cell average flux, an adjustment factor is introduced as following to satisfy Eq. (4.8).

$$\varepsilon_m = \frac{\bar{\varphi}_m^{het}}{\bar{\varphi}_m^{\hom}} \tag{4.9}$$

Then, the surface angular fluxes are adjusted accordingly using the surface angular flux of the pilot solution as:

$$\varphi_{i-1/2,m}^{+} = \varphi_{i-1/2,m}^{\hom} \times \varepsilon_m, \quad \varphi_{i+1/2,m}^{-} = \varphi_{i+1/2,m}^{\hom} \times \varepsilon_m . \tag{4.10}$$

Finally, the angular discontinuity factors are then determined as:

$$f_{i-1/2,m}^{+} = \frac{\varphi_{i-1/2,m}^{het}}{\varphi_{i-1/2,m}^{+}}, \quad f_{i+1/2,m}^{-} = \frac{\varphi_{i+1/2,m}^{het}}{\varphi_{i+1/2,m}^{-}} . \tag{4.11}$$

By substituting Eqs. (4.9) through (4.11) into Eq. (4.8), it is possible to show that the requirement for the cell average angular flux is indeed conserved as:

$$\begin{aligned} \varphi_m &= \frac{1}{2}\left(\frac{\varphi_{i-1/2,m}^{het}}{f_{i-1/2,m}^{+}} + \frac{\varphi_{i+1/2,m}^{het}}{f_{i+1/2,m}^{-}} \right) = \frac{1}{2}\left(\varphi_{i-1/2,m}^{\hom} + \varphi_{i+1/2,m}^{\hom} \right) \varepsilon_m \\ &= \varphi_m^{\hom} \frac{\bar{\varphi}_m^{\text{het}}}{\varphi_m^{\hom}} = \bar{\varphi}_m^{\text{het}} . \end{aligned} \tag{4.12}$$

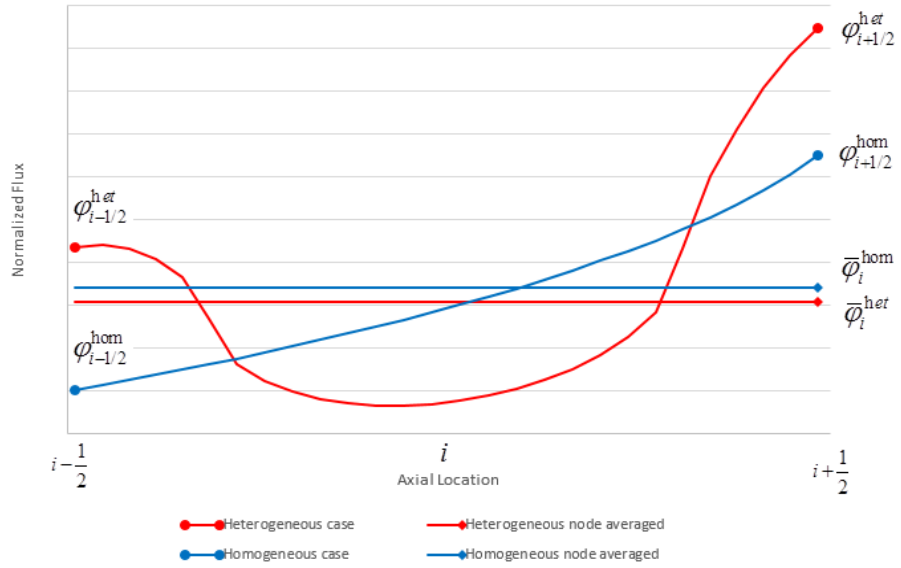

(a) Before applying the adjustment factor ε_m

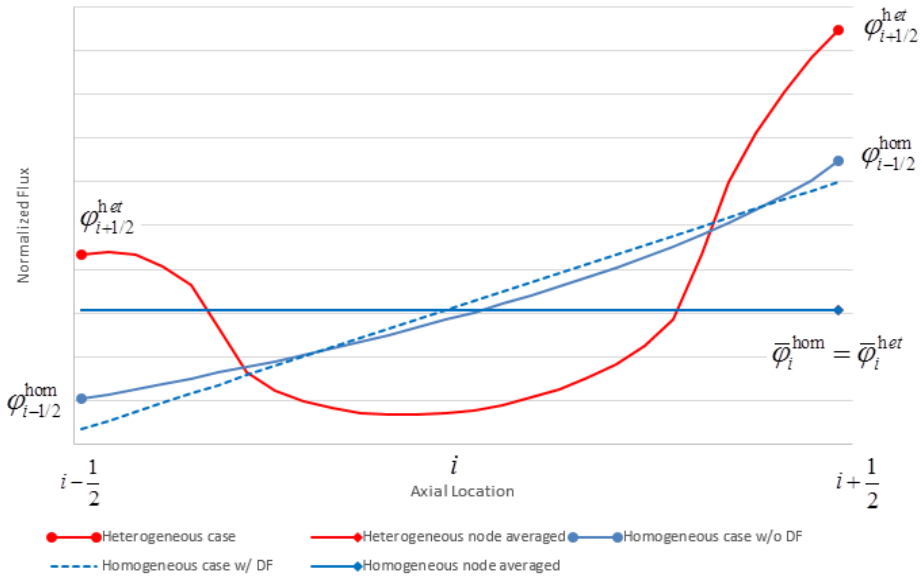

(b) After applying the adjustment factor ε_m

Fig. 4-4 Discrepancy between Heterogeneous and Homogeneous Flux

It can also be seen in Fig. 4-4(b). After applying the adjustment factor, the homogenized cell average angular flux is equal to the heterogeneous cell average angular flux.

The second solution of the homogenized problem constructed now by applying the angular flux discontinuity factors determined by Eq. (4.11) can be fully consistent with that of the reference heterogeneous problem.

4.1.3 Construction of Equivalent Coarse Mesh Formulation

Previously, the angular discontinuity factor and homogenized cross section by the flux-volume weighting method are applied to the one-dimensional discrete ordinates equation. To verify the performance of the homogenization method, the verification is carried out as follows

(1) Performs heterogeneous calculation and pilot calculation for the homogenized problem without the angular discontinuity factors in a simplified single assembly geometry.
(2) Calculates angular discontinuity factors and homogenized cross sections from the above derivations.
(3) Performs homogenized calculation in the assembly geometry using the above homogenized parameters.

(4) Compares the homogeneous calculation result with that of the heterogeneous reference calculation in the assembly geometry.
(5) Evaluates performance of the homogenization method based on the discrepancy between homogeneous and heterogeneous (reference) calculations.

The homogenization methods described in the previous section can exactly reproduce the reference solution, so there will be no discrepancy between the homogenized and heterogeneous calculations.

The calculations are performed in one-dimensional slab geometry that represents simplified but typical situation of LWR assembly calculations. Calculation configuration is shown in Fig. 4-5.

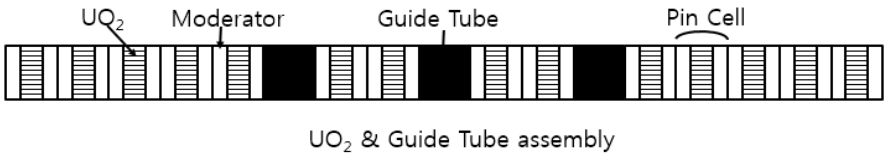

Fig. 4-5 Calculation Configuration of the 1-D Slab Geometry

The calculation configuration simulates assembly geometry that two-different types of pin cells are arranged. Thicknesses of fuel and moderator are 0.732 cm and 0.264 cm, thus pin cell pitch is 1.26 cm. Number of energy group of this calculation is seven group and

reflective boundary condition is used at left and right boundary. Each heterogeneous pin consists of 28 heterogeneous meshes and cell-homogenized parameters are generated after the heterogeneous calculation so that homogenized problem is made up of 17 homogenized meshes.

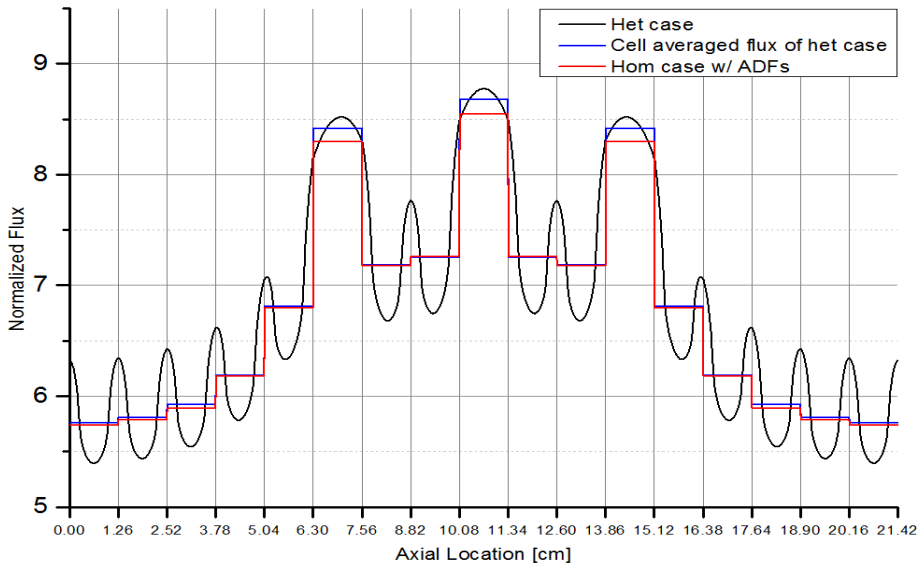

Fig. 4-6 Thermal Flux Distribution of the Single Assembly Problem

Table 4-1 Comparison of the k_{inf} and Fission Source Error of the Single Assembly

	Heterogeneous prob.	Homogeneous prob.	Homogeneous prob. w/ AnDF
k_{inf}	1.31129	1.31618[283 pcm]	1.31195 [38 pcm]
Err. F. S.[%]		1.01	0.19

Fig. 4-6 and Table 4-1 show the results of UO_2 & Guide Tube assembly problem. The angular discontinuity factors reduce the homogenization error compared to the results of the homogeneous calculation without the discontinuity factors. But, there is undesirable error between absorber and fuel pin cell.

Because there is no mistake in defining the angular discontinuity factors to reproduce the heterogeneous reference solution, fixed source problem for the homogenized problem is constructed to verify the suitability of the homogenized total cross section $\bar{\Sigma}_t$. The homogenized problem should be consistent with the heterogeneous problem when the incoming angular flux and source term of the heterogeneous problem are directly used in the homogenized problem, if there is no problem for using the homogenized total cross section.

When the fixed source problem for the homogenized problem is constructed as:

$$\frac{\mu_m}{\Delta x_i}(\varphi^{het}_{i+1/2,m} - \varphi^{het}_{i-1/2,m}) + \bar{\Sigma}_t \varphi_m = q^{het}_m \tag{4.13}$$

the homogeneous cell average angular flux should be equal to the heterogeneous cell average angular flux as:

$$\varphi_m = \frac{q^{het}_m \Delta x_i - \mu_m(\varphi^{het}_{i+1/2,m} - \varphi^{het}_{i-1/2,m})}{\bar{\Sigma}_t \Delta x_i} = \bar{\varphi}^{het}_m . \tag{4.14}$$

The same verification is performed for the fixed source problem. Calculation configuration and condition is equal to the previous verification problem. Fig. 4-7 and table 4-2 show the result of the problem. There is a slight difference between the heterogeneous and homogenized calculation as shown in Fig. 4-7 but there shouldn't be any difference. Because the incoming angular flux and source term are calculated from the heterogeneous problem and used directly in the homogenized problem. Consequently, the result shows that it is not suitable to use the homogenized total cross section.

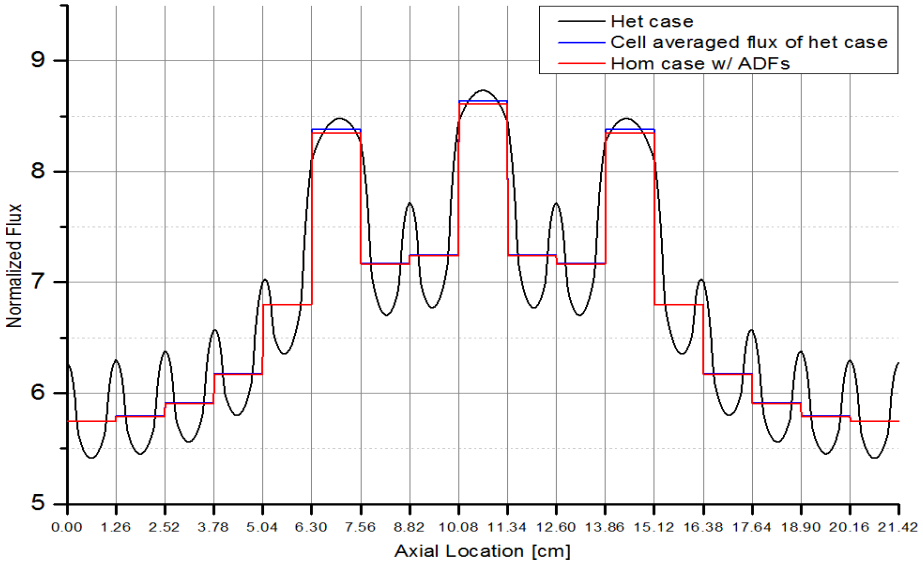

Fig. 4-7 Thermal Flux Distribution of the Fixed Source Problem

Table 4-2 Comparison of the Fission Source Error of the Fixed Source Problem

	Heterogeneous prob.	Homogeneous prob.	Homogeneous prob. w/ AnDF
Err. F. S.[%]	-	1.01	4.37E-03

Finally, angle dependent homogenized total cross section is defined to make the homogenized problem fully consistent with the heterogeneous problem.

$$\overline{\Sigma}_{t,i,m} = \frac{\sum_{i \in V} \Sigma_{t,i}^{het} \varphi_{i,m}^{het} V_i}{\sum_{i \in V} \varphi_{i,m}^{het} V_i} . \quad (4.15)$$

The difference between the homogenized total cross section with no angle dependency and angle dependent homogenized total cross section is checked for same position and energy group. Table 4-3 shows difference between the two homogenized total cross sections.

Table 4-3 Comparison of the Two Homogenized Total Cross Sections

Cell	Group	$\overline{\Sigma}_t$	Angle	$\overline{\Sigma}_{t,m}$	Difference [%]
1	7	1.54419	1	1.45849	5.55
			2	1.46143	5.36
			3	1.46543	5.10
			4	1.47116	4.73
			5	1.48007	4.15
			6	1.49582	3.13
			7	1.53137	0.83
			8	1.70309	10.29
			…	…	…

According to the angle variation, there is maximum 10% difference between the two homogenized total cross section. In the heterogeneous problem, a heterogeneous cell is divided by several

meshes. Because of that reason, the angle dependency can be neglected and the homogenized total cross section with no angle dependency can be used. On the contrary, the homogenized cell is directly used as computational mesh in the homogenized problem. So, length of the mesh becomes longer and the angle dependency cannot be neglected. Therefore, the angle dependent homogenized total cross section should be used in the homogenized problem to reproduce the heterogeneous reference solution perfectly.

After applying the angular discontinuity factors and angle dependent homogenized total cross section, the verification is carried out again for the eigenvalue problem. Fig. 4-8 and Table 4-4 show the results of the assembly problem with the angular discontinuity factors and angle dependent homogenized total cross section.

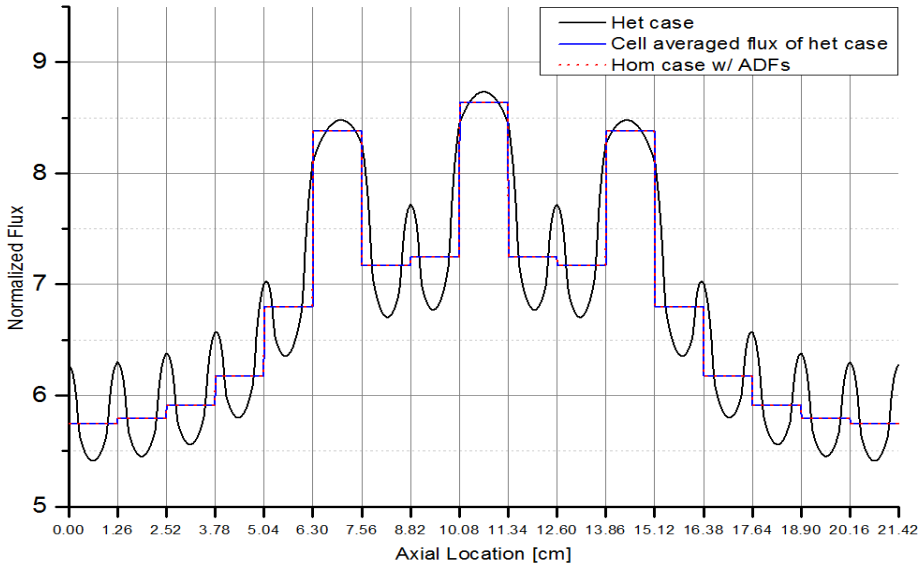

Fig. 4-8 Thermal Flux Distribution of the Eigenvalue Problem

Table 4-4 Comparison of the k_{inf} and Fission Source Error of the Single Assembly Problem

	Heterogeneous prob.	Homogeneous prob.	Homogeneous prob. w/ AnDF
k_{inf}	1.31129	1.31618[283 pcm]	1.31129 [0 pcm]
Err. F. S.[%]	-	1.01	1.39E-05

There is no difference between the heterogeneous and homogenized problem with the angular discontinuity factors. The homogeneous solution is fully consistent with the heterogeneous solution of the

eigenvalue problem by using the angular discontinuity factors and angle dependent homogenized total cross section.

4.1.4 Angular Discontinuity Factors in Two-dimensional Discrete Ordinates Equation

After applying the angular discontinuity factors to one-dimensional discrete ordinates equation, extension of the angular discontinuity factors to two-dimensional is performed. The derivation is straightforward in the two-dimensional case compared to the one-dimensional case.

There are several points in defining the discontinuity factors in the 2-D. In the 2-D case, the angular discontinuity factors are defined not only for the left and right cell boundaries (west and east face), but also for south and north cell boundaries. Because the node average flux is related to angular flux of each direction, the node average flux is defined by the angular discontinuity factors depending on the angular directions.

The 2-D discretized Boltzmann transport equation is given as:

$$\frac{\xi_m}{\Delta x_i}(\varphi_{i+1/2,m}-\varphi_{i-1/2,m})+\frac{\eta_m}{\Delta y_j}(\varphi_{j+1/2,m}-\varphi_{j-1/2,m})+\bar{\Sigma}_{tm}\varphi_m=q_m\,. \quad (4.16)$$

Now let's define a 2-D homogenized node (coarse mesh) l as depicted in Fig. 4-9.

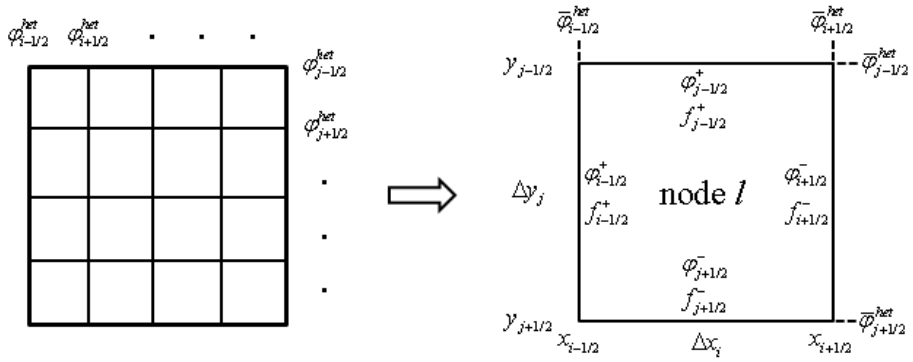

Fig. 4-9 Homogenized Node l in 2-D case

The 2-D spatial neutron balance equation for the node l is obtained by integrating Eq. (4.16) over the node l as:

$$\xi_m(\varphi_{i+1/2,m}-\varphi_{i-1/2,m})\Delta y_j+\eta_m(\varphi_{j+1/2,m}-\varphi_{j-1/2,m})\Delta x_i+\bar{\Sigma}_{tm}V_l\varphi_m=q_mV_l\,. \quad (4.17)$$

The homogenized cross section denoted by the overbar symbol is determined by the angular flux-volume weighting method. Note that the homogenized total cross section has angle dependency.

To preserve the net current at each surface, the homogeneous angular surface flux should be equal to the heterogeneous angular surface flux.

$$\xi_m(\varphi^{het}_{i+1/2,m}-\varphi^{het}_{i-1/2,m})\Delta y_j+\eta_m(\varphi^{het}_{j+1/2,m}-\varphi^{het}_{j-1/2,m})\Delta x_i+\bar{\Sigma}_{tm}V_l\varphi_m=q_mV_l. \quad (4.18)$$

This current conservation can be achieved by introducing flux discontinuity at the cell interface described in the 4.1.2 section. By definition of the DF, the flux continuity condition at the cell interface is defined as:

$$\varphi^{het}_{i-\frac{1}{2},m}=f^{-}_{i-\frac{1}{2},m}\varphi^{-}_{i-\frac{1}{2},m}=f^{+}_{i-\frac{1}{2},m}\varphi^{+}_{i-\frac{1}{2},m},\quad \varphi^{het}_{j-\frac{1}{2},m}=f^{-}_{j-\frac{1}{2},m}\varphi^{-}_{j-\frac{1}{2},m}=f^{+}_{j-\frac{1}{2},m}\varphi^{+}_{j-\frac{1}{2},m}. \quad (4.19)$$

With the diamond difference relation, the node average angular flux in node l is expressed by the flux value at the midpoint of the cell.

$$\begin{aligned}\varphi_m&=\frac{1}{2}(\varphi^{+}_{i-1/2,m}+\varphi^{-}_{i+1/2,m})=\frac{1}{2}\left(\frac{\varphi^{het}_{i-1/2,m}}{f^{+}_{i-1/2,m}}+\frac{\varphi^{het}_{i+1/2,m}}{f^{-}_{i+1/2,m}}\right)\\ \varphi_m&=\frac{1}{2}(\varphi^{+}_{j-1/2,m}+\varphi^{-}_{j+1/2,m})=\frac{1}{2}\left(\frac{\varphi^{het}_{j-1/2,m}}{f^{+}_{j-1/2,m}}+\frac{\varphi^{het}_{j+1/2,m}}{f^{-}_{j+1/2,m}}\right).\end{aligned} \quad (4.20)$$

By using Eqs. (4.18) and (4.20), the node average angular flux in node

l for $\xi_m > 0$ and $\eta_m > 0$ is obtained as:

$$\varphi_m = \frac{q_m V_l + \xi_m (1 + \frac{f^-_{i+1/2,m}}{f^+_{i-1/2,m}}) \varphi^{het}_{i-1/2,m} \Delta y_j + \eta_m (1 + \frac{f^-_{j+1/2,m}}{f^+_{j-1/2,m}}) \varphi^{het}_{j-1/2,m} \Delta x_i}{2\xi_m f^-_{i+1/2,m} \Delta y_j + 2\eta_m f^-_{j+1/2,m} \Delta x_i + \bar{\Sigma}_{tm} V_l}. \quad (4.21)$$

In sweeping through the spatial meshes toward the positive direction, Eq. (4.20) is used to define the east and south boundary angular flux of node l.

$$\begin{aligned} \varphi^{het}_{i+1/2,m} &= 2 f^-_{i+1/2,m} \varphi_m - \frac{f^-_{i+1/2,m}}{f^+_{i-1/2,m}} \varphi^{het}_{i-1/2,m} \\ \varphi^{het}_{j+1/2,m} &= 2 f^-_{j+1/2,m} \varphi_m - \frac{f^-_{j+1/2,m}}{f^+_{j-1/2,m}} \varphi^{het}_{j-1/2,m} \end{aligned} . \quad (4.22)$$

Using the current relation and reaction rate conservation given by Eqs. (4-18) through (4.22) together with the angle dependent homogenized total cross section defined in Eq. (4.15), the spatial neutron balance in each cell can be guaranteed and thus the resulting solution of the homogenized problem can be the same as the original solution as far as the average angular fluxes (and the eigenvalue as well) are concerned. In the real applications, the heterogeneous reference

solution to be used in Eqs. (4.18) through (4.22) is replaced by a partially converged heterogeneous S_N solution which is to be iteratively updated.

Until now, the extension of this approach to 2-D problem is achieved. Effect of the angular discontinuity factors in 2-D will be evaluated in chapter 5.

4.2 Acceleration Scheme Employing Angular Discontinuity Factors

The homogenized problem which is fully consistent with the heterogeneous reference problem is constructed by using the angular discontinuity factors and angle dependent total cross section in the previous sections. It is necessary to accelerate the S_N eigenvalue calculation. In this section, acceleration scheme employing the angular discontinuity factors will be described.

4.2.1 Alternating calculation procedure

An alternating calculation procedure involving the fine mesh S_N solution and the coarse S_N or S_2 solutions is established for the

acceleration of the outer iterations as:

(1) Perform the power iteration for the fine mesh heterogeneous to achieve partial convergence.
(2) Generate the angle dependent homogenized cross sections for coarse meshes using the partially converged fine mesh heterogeneous solution.
(3) Perform the pilot calculation for the coarse mesh homogenized problem without the angular discontinuity factors.
(4) Determine the angle dependent surface discontinuity factors using the heterogeneous and homogeneous solution.
(5) Perform the power iteration for the coarse mesh homogenized problem with tighter convergence.
(6) Adjust the source term of the heterogeneous problem by the method of modulation using the coarse mesh average fluxes and the shape function for the heterogeneous problem stored in the previous heterogeneous calculation.
(7) Repeat steps 1 through 6 until overall convergence.

4.2.2 Prolongation

In each heterogeneous calculation, the regional source distribution and the incoming angular fluxes at the problem boundary are to be given. Since only the cell average values of the scalar flux and the surface average angular flux are available from the homogenized problem, prolongation operations are needed. This can

be performed by using the spatial and angular shapes that are determined at the previous heterogeneous calculation. Specifically, the regional scalar flux and the boundary outgoing angular fluxes are updated using the following relations.

$$\phi_g^{k,l+\frac{1}{2}} = \frac{\phi_g^{k,l}}{\bar{\phi}_g^{i,l}} \bar{\phi}_g^{i,l+\frac{1}{2}}$$
$$\varphi_{g,m}^{p,l+\frac{1}{2}} = \frac{\varphi_{g,m}^{p,l}}{\bar{\varphi}_{g,m}^{p,l}} \bar{\varphi}_{g,m}^{p,l+\frac{1}{2}} \tag{4.23}$$

where $\varphi_{g,m}^{p,l}$ is the angular flux of group g and angle m at a point p on a boundary surface s of a boundary cell i at the l-th heterogeneous S_N update. The incoming angular flux for the heterogeneous calculation is determined from the outgoing angular flux of Eq. (4.23) and boundary condition.

4.2.3 Nonlinear Iteration Control

In the homogeneous calculation with the angular discontinuity factors, periodical updates of the homogenized parameters from the heterogeneous calculation are required and this is referred to as the nonlinear iteration. Since it is not necessary to generate a fully

converged solution for each set of homogenized parameters, there should be efficient control logic to derive the homogeneous calculation by monitoring convergence. In this acceleration scheme, partial convergence of each homogeneous solution is determined by monitoring the relative residual which is the $l2$ norm of the residual vector of the linear system consisting of the multigroup homogenized cell balance equation. Specifically, the element of the residual vector is defined as:

$$r^n_{m,g,i} = \xi_m(\varphi^n_{m,g,i+1} - \varphi^n_{m,g,i})\Delta y + \eta_m(\varphi^n_{m,g,\mathrm{j}+1} - \varphi^n_{m,g,j})\Delta x + \bar{\Sigma}_{tm}\varphi^n_{m,g}V_l - \lambda^n q^n_{m,\mathrm{g}}V_l \quad (4.24)$$

where indices n, g and ij are the iteration, group and cell numbers, respectively and $q^n_{m,g}$ is the total source within the volume of cell at the n-the iteration step.

4.2.4 Condensation of higher order S_N ordinates

In the Discrete Ordinates Method, the continuous angular variation is approximated using a finite set of discrete directions with corresponding directional weighting factors. The most commonly used

quadrature set is the S_N quadrature, also referred to as level-symmetric quadrature, where total number of direction is defined as:

$$M = N(N+2) \tag{4.25}$$

where indices M and N are the number of segments and different cosines. In order to obtain accurate solutions, higher order S_N quadrature is needed in the heterogeneous S_N calculation. But, it can increase the computational burden of the homogeneous calculation and total computing time. To reduce the computational burden of the homogeneous calculation, the higher order S_N quadrature is condensed into the S_2 quadrature in the homogeneous calculation. If the higher order S_N quadrature can be condensed into the S_2 quadrature in the homogeneous calculation, the computational burden and computing time of the homogeneous problem can be significantly reduced. For the S_2 quadrature, there is only one direction per quadrant in 2-D geometry. So, it is possible to condense the higher order S_N quadrature into the S_2 quadrature preserving the scalar flux and current.

To define the AnDFs and homogenized cross sections in the S_2 quadrature, the heterogeneous angular surface flux and angular average flux in the higher order S_N quadrature should be preserved in the S_2 quadrature. The heterogeneous angular surface flux and angular average flux for the S_2 quadrature is obtained by preserving the current at each surface and the scalar flux at each cell in each quadrant in 2-D geometry. Before the homogeneous calculation, the heterogeneous angular surface flux and angular average flux for S_2 quadrature are calculated using the following relations.

$$\begin{aligned}\varphi^{S_2}_{i\pm\frac{1}{2},M} &= \frac{J^{S_N}_{i\pm\frac{1}{2},M}}{w^{S_2}_M \xi^{S_2}_M} = \frac{\sum_{m\in M} w^{S_N}_m \xi^{S_N}_m \varphi^{S_N}_{i\pm\frac{1}{2},m}}{w^{S_2}_M \xi^{S_2}_M} \\ \varphi^{S_2}_{i,M} &= \frac{\phi^{S_N}_{i,M}}{w^{S_2}_M} = \frac{\sum_{m\in M} w^{S_N}_m \varphi^{S_N}_{i,m}}{w^{S_2}_M}\end{aligned} \tag{4.26}$$

where the $\varphi^{S_2}_{i\pm\frac{1}{2},M}$ is a heterogeneous angular surface flux for S_2 quadrature, $J^{S_N}_{i\pm\frac{1}{2},M}$ is a heterogeneous surface current for higher order S_N quadrature, $\varphi^{S_2}_{i,M}$ is a heterogeneous angular average flux for S_2

quadrature, $\phi_{i,M}^{S_N}$ is a heterogeneous scalar flux for higher order S_N quadrature and M is represented the number of segments in quadrant for higher order S_N quadrature.

By using the two parameters, the AnDFs and homogenized cross sections are defined before the homogeneous calculation. Then, the homogeneous calculation applying S_2 quadrature is performed. The consistency check for the condensation of the higher order S_N quadrature is achieved for the C5G7 benchmark problem. And four quarter core problems are calculated to examine performance of the method in terms of the computing time. The result is attached in the chapter 5.4.

Chapter 5. Performance Examinations

The performance of the acceleration scheme is examined for various test problems ranging from single assembly to typical PWR problems. The assembly configurations and the 7 group cross section data for each composition are taken from the C5G7 benchmark problem which involved three types of assemblies. For each problem, the reference solution is generated by converging the solution very tightly and this solution is used to compute the true error of each solution iterate. The unaccelerated case which employed only the heterogeneous S_N calculations and the power iteration was performed in parallel with the homogenized case with the angular discontinuity factors to ensure solution convergence and to compare the performance.

5.1 Effect of the Angular Discontinuity Factors

Before examining the performance of the angular flux discontinuity factors based S_N acceleration scheme, the consistency

between the heterogeneous problem and homogenized problem is checked with the C5G7 benchmark problem shown in Fig. 5-1.

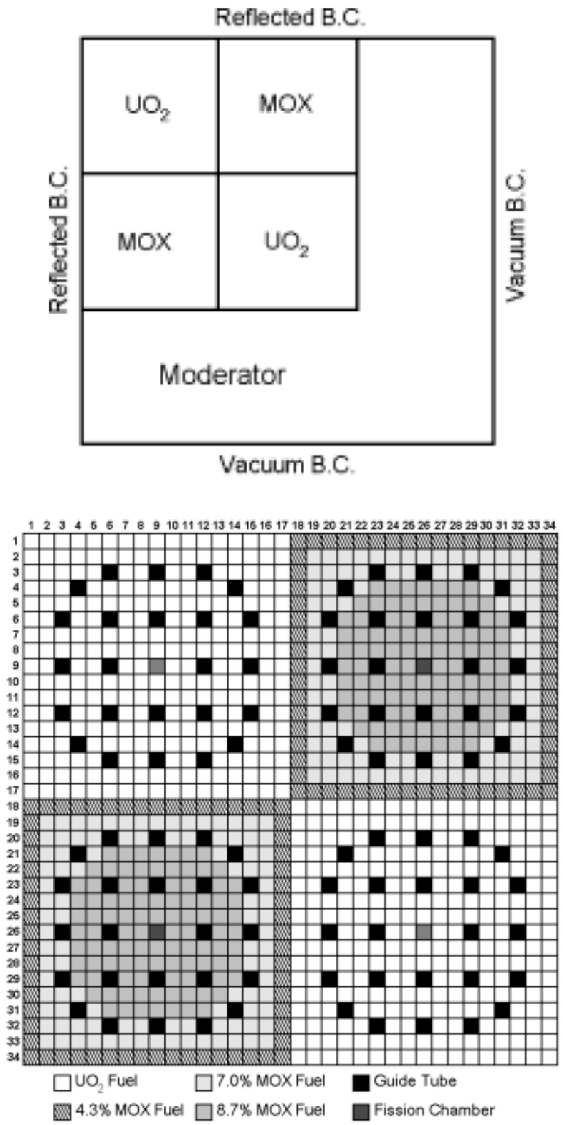

Fig. 5-1 Configuration of the C5G7 Benchmark Problem

The C5G7 benchmark problem has three types of heterogeneous assembly into which heterogeneous fuel pins and guide tubes are placed as shown in Fig. 5-1. Each fuel pin cell in the assembly consists of 6x6 heterogeneous fine meshes. The fuel composition is assigned to the interior 20 meshes and the moderator composition to outside meshes surrounding the fuel. The width of the assembly is 21.42 cm and width of the coarse mesh for the homogenized problem is 1.26cm while that of the fine mesh for the reference heterogeneous problem is 0.21 cm so that 36 fine meshes are assigned to each coarse mesh. Seven sets of seven group cross sections are used. The k-effectives of the reference heterogeneous solution, the solutions for the homogenized problems with and without the angular discontinuity factors are listed in Table 5-1 together with the errors in the fission source distribution.

Table 5-1 Effects of the Angular Discontinuity Factors

	Heterogeneous prob.	Homogeneous prob.	Homogeneous prob. w/ AnDF
k_{eff}	1.19088	1.17111	1.19088
k_{eff} Error [pcm]	-	1977	0
Err. F. S.[%]	-	7.5	5.4E-03

It is noted that the large errors such as about 2000 pcm in k_{eff} and 8% in fission source distribution for the case without the angular discontinuity factors disappear with the use of the angular discontinuity factors. Consequently, it is able to verify that the homogenized problem is constructed fully consistent with the heterogeneous problem by using the angular discontinuity factors.

5.2 Convergence for the Base Case

In this section, the solution convergence of the accelerated case is examined for the base case. The base case is the original 3x3 C5G7 benchmark problem as depicted in Fig. 5-1.

The convergence of k_{eff} for the base case is shown in Fig. 5-2. The eigenvalue is updated at every outer iteration of homogeneous

calculation with the angular discontinuity factors. As shown in Fig. 5-2, the eigenvalue stabilizes very quickly around the converged value (1.19088) only after three heterogeneous S_N updates.

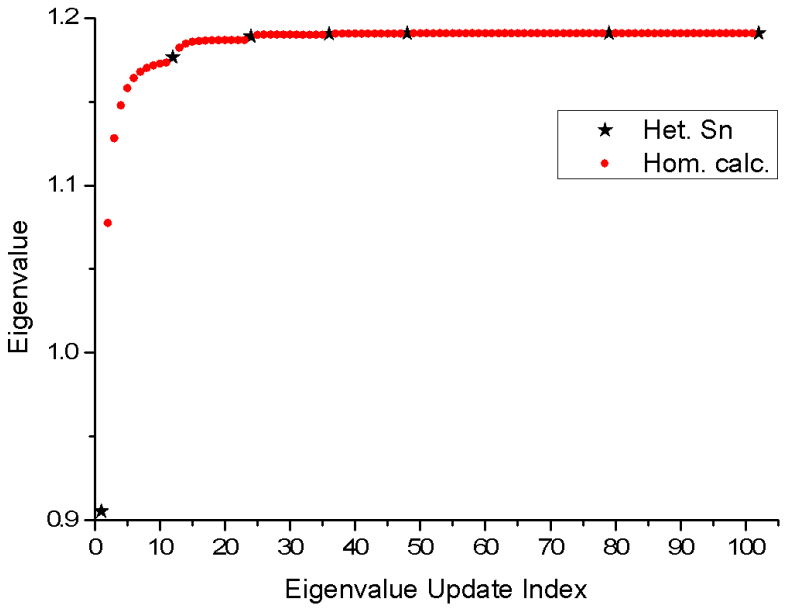

Fig. 5-2 Convergence of Eigenvalue for the Base Case

Compared with the unaccelerated case as shown in Fig. 5-3, the accelerated case is roughly 7 times more effective in that only 7 heterogeneous S_N updates are required to reach the true global fission source error of 10^{-5} whereas about 47 heterogeneous S_N updates are for the unaccelerated case.

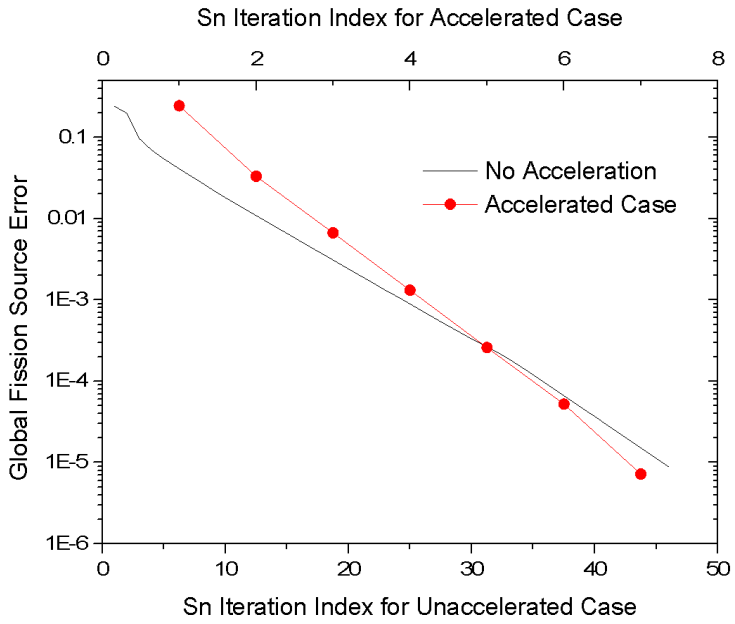

Fig. 5-3 Global Fission Source Error Reduction Behavior

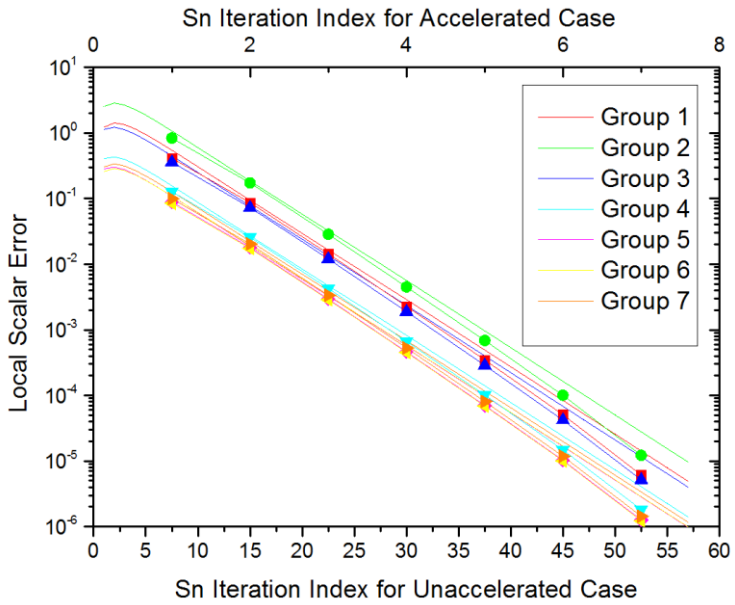

Fig. 5-4 Convergence of Local Scalar Flux

The local solution converges indeed to the same value as shown in Fig. 5-4 which shows regional group scalar fluxes at an interior cell.

The rapid essential convergence shown in Fig. 5-2 through 5-4 and the steady exponential error reduction in the later iteration steps mean that only a few heterogeneous S_N calculations are sufficient to catch up most of the spectral, spatial coupling and transport effects. This would be possible because fission and scattering source distributions determined from the prior homogeneous calculation with the angular discontinuity factors provides much better source information than what can be obtained with the heterogeneous S_N alone.

5.3 Convergence Sensitivity

The sensitivity of the convergence characteristics of the accelerated case on core size is examined. In this sensitivity study, the number of outer iterations between the normal S_N power iteration case and the accelerated case is compared to examine the performance of the acceleration of S_N power iteration. For the two calculations, the

number of outer iterations required to reach the fission source convergence of 10^{-5} is considered.

The dependence of the acceleration on the core size is of particular interest so that five quarter-core problems are constructed with different number of fuel assemblies. The numbers of fuel assemblies along one axis are 1, 3, 5, 7 and 9, respectively for the five quarter-core problems. The second case (3 fuel assemblies along the axis) is the same as the C5G7 benchmark problem. Similarly to this core, the cores are reflected with a row of reflector except for the first core. The results for the five cores are listed in Table 5-2. Fig. 5-5 shows the reduction behavior of the global fission source error for different core sizes. N_x in the Table 5-2 denotes the number of assemblies placed in the horizontal direction.

Table 5-2 Acceleration Performance for Core Problem

Problem Size		Dominance Ratio	# of Fine Mesh S_N Iterations	
N_x	# of FAs		Unaccelerated	Accelerated
1	1	0.42275	15	6
3	4	0.78954	46	7
5	16	0.92588	121	7
7	36	0.96287	224	7
9	64	0.97802	352	7

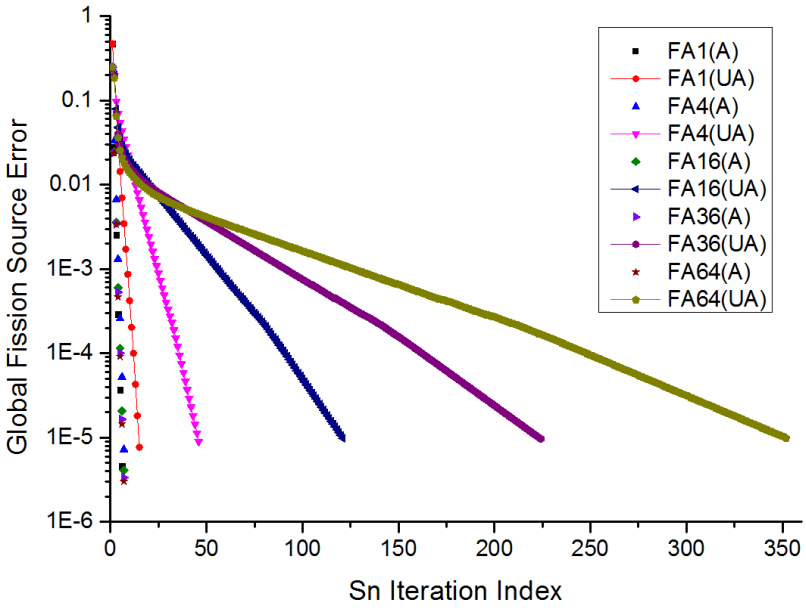

Fig. 5-5 Global Fission Source Error Reduction Behavior

A very important acceleration characteristics is noted in Table 5-2. Namely, the convergence of the accelerated case doesn't reveal any

significant dependence on the problem size which would affect the dominance ratio in that the number of fine mesh S_N power iteration stays around 7 whereas the unaccelerated case suffers significantly from the increased core size as shown in Table 5-2. As indicated by the dominance ratio which is obtained as the ratio of the true errors of the two successive iterates the eigenvalue separation becomes very small as the problem size increases. In the physical point of view, it takes much longer to propagate the boundary information to the core interior in the plain power iteration case for a larger core. However, with the homogeneous calculation, the boundary information is instantaneously propagated to the interior so that rapid convergence is possible. Due to this fact, the speed up is over 17 for the practical core cases. For the largest problem here, even a speedup of 50 is achieved.

5.4 Computing Time

The computing times measured are listed in Table 5-3. In the test cases, S_8 approximation is used. And the width of the coarse mesh for the homogenized problem is 1.26 cm while that of the fine mesh for

the reference heterogeneous problem is 0.21 cm so that a coarse mesh consists of one heterogeneous pin.

Table 5-3 Comparison of Computing Time for Core Problem

Problem Size		Dominance Ratio	Computing Time, sec	
N_x	# of FAs		Unaccelerated	Accelerated
1	1	0.42275	117	59
3	4	0.78954	6317	1264
5	16	0.92588	92669	7333
7	36	0.96287	379381	22538
9	64	0.97802	983959	50886

The speedup is about 19 for the 9x9 quarter core problem. But it is unsatisfactory result in terms of the reduction of computational time. So, computing time breakup is performed for the three primary modules of the 2-D S_N code to check fraction of the computing time for each module. Table 5-4 shows comparison of the computing time breakup.

Table 5-4 Comparison of Computing Time Breakup

Module	C5G7 (3x3, 4 FAs)		Typical PWR (9x9, 64 FAs)	
	CPU Time, sec	Fraction, %	CPU Time, sec	Fraction, %
Pilot Calc.	0.77	0.07	11.33	0.02
Hom w/ AnDF	262.23	24.17	34883.66	68.55
S_N Calc	821.79	75.76	15991.62	31.43
Total	1084.79		50886.61	

The time for the heterogeneous S_N calculation is dominating by taking more than 75% of the total computation time for the base case. But a fraction of the computing time for the homogeneous calculation with angular discontinuity factors increases when the core size is larger. It is because that computational burden for inner iteration increases in the homogeneous calculation. So, there is motivation for employing coarser level homogeneous formulation to reduce the computational burden in homogeneous calculation.

For 6x6 C5G7 problem, sensitivity of computing time on the coarse mesh size is examined. The numbers of heterogeneous pin cell that forms homogenized coarse mesh are 1, 2, 3 and 6 for the problem. Table 5-5 shows comparison of computing time breakup in terms of

the coarse mesh size.

Table 5-5 Comparison of Computing Time Breakup in terms of the Coarse Mesh Size

Module	Unaccelerated		Accelerated (one pin cell)	
	CPU Time, sec	Fraction, %	CPU Time, sec	Fraction, %
Pilot Calc.	-	-	3.86	0.03
Hom w/ AnDF	-	-	6800.04	52.58
S_N Calc	175651.25	100	6128.73	47.39
Total	175651.25		12932.63	

Module	Accelerated (two pin cells)		Accelerated (three pin cells)	
	CPU Time, sec	Fraction, %	CPU Time, sec	Fraction, %
Pilot Calc.	1.18	0.02	0.71	0.01
Hom w/ AnDF	2182.23	40.97	1025.22	8.88
S_N Calc	3143.05	59.01	10514.68	91.11
Total	5326.46		11540.61	

Module	Accelerated (six pin cells)	
	CPU Time, sec	Fraction, %
Pilot Calc.	0.23	0.001
Hom w/ AnDF	457.47	2.802
S_N Calc	15866.18	97.197
Total	16323.88	

When coarser mesh is used, less computing time in the homogeneous calculation with angular discontinuity factors is achieved. Computational burden of the homogeneous calculation decreases but that of heterogeneous S_N calculation increases. Because the number of heterogeneous S_N outer iteration increases when coarser mesh is used. As a result, the total computing time increases though the computational burden of the homogeneous calculation decreases. It is important to determine proper coarse mesh size to achieve better performance in terms of the computing time. For the 6x6 C5G7 problem, using coarse mesh composed of two heterogeneous pin cell shows best performance. Compared to one heterogeneous pin cell case, the total computing time is reduced in over half.

The table 5-6 shows the computing time and speedup varying with the core sizes. In this calculation, several heterogeneous pin cell sized coarse mesh is used in the homogenized problem. The speedup is about 84 for the 9x9 quarter core problem. Compared to one heterogeneous pin cell sized coarse mesh case, computing time for the

accelerated case is reduced in over fourth.

Table 5-6 Comparison of Computing Time and Speedup for Core Problem

Problem Size		Computing Time, sec		Speedup
N_x	# of FAs	Unaccelerated	Accelerated	
1	1	117	59	1.9
3	4	6317	1085	5.8
5	16	92669	5326	17.4
7	36	379381	9429	40.2
9	64	983959	11718	83.9

So far, coarser level homogeneous formulation is applied to reduce the computational burden and computing time in homogeneous calculation.

Furthermore, condensation of higher order S_N ordinates is achieved for the same objectives. Before examining the performance of the S_2 approximation, the consistency between the heterogeneous calculation and the homogenized calculation employing the S_2 approximation is checked with the base case. The k-effectives of the reference heterogeneous solution, the solutions for the homogenized

problems with and without the S_2 approximation are listed in Table 5-7 together with the errors in the fission source distribution.

Table 5-7 Consistency check for the S_2 Quadrature

	Heterogeneous prob.	Hom. w/ AnDF (S_8)	Hom. w/ AnDF (S_2)
k_{eff}	1.19088	1.19088	1.19088
k_{eff} Error [pcm]	-	0	0
Err. F. S.[%]	-	5.4E-03	1.4E-02

The homogenized problem reproduces the reference heterogeneous solution although S_2 approximation is used in the homogeneous calculation.

To examine performance of the S_2 approximation in terms of the computing time, four quarter core problems are calculated. The S_8 approximation is used in the heterogeneous calculation and S_2 approximation is used in the homogeneous calculation. The results are listed in Table 5-8 and 5-9.

Table 5-8 Comparison of Total Computing Time between S_8 Quadrature and S_2 Quadrature

Problem Size		Computing Time, sec (N_{iter})		
N_x	# of FAs	Unaccelerated	Accelerated (S_8)	Accelerated (S_2)
3	4	6317 (46)	1264 (7)	1223 (7)
5	16	92669 (121)	7333 (7)	5372 (11)
7	36	379381 (224)	22538 (7)	13185 (11)
9	64	983959 (352)	50886 (7)	33322 (12)

Table 5-8 shows comparison of total computing time for original and S_2 approximation scheme. The total computing time is reduced by using the S_2 approximation in the homogeneous calculation. But, the number of outer iteration increases because of inaccurate solution update calculated in the homogeneous calculation using the S_2 approximation.

Table 5-9 shows comparison of computing time breakup between the two schemes for 7x7 C5G7 benchmark problem. The fraction of computing time for the homogeneous calculation is significantly reduced by using the S_2 approximation in the homogeneous calculation.

Table 5-9 Comparison of Computing Time Breakup between Two Schemes for 7x7 C5G7 benchmark problem

Module	Accelerated Case (S_8)		Accelerated Case (S_2)	
	CPU Time, sec	Fraction, %	CPU Time, sec	Fraction, %
Pilot Calc.	9	0.04	1	0.01
Hom w/ AnDF	10088	44.76	1041	7.89
S_N Calc	12441	55.2	12143	92.1
Total	22538		13185	

Consequently, it is able to reduce the computational burden of the homogeneous calculation by using the S_2 approximation while retaining the accuracy of the heterogeneous solution.

Chapter 6. Summary and Conclusions

In order to accelerate heterogeneous fine mesh S_N calculations, a coarse mesh S_N formulation employing the angular flux discontinuity factors (AnDFs) was derived. The homogenized problem was constructed by employing the angular flux discontinuity factors as well as the angle dependent total cross sections. The scheme to calculate the AnDFs properly was developed by employing the solution of the pilot coarse mesh problem in which AnDFs are not used. By using those proper homogenization parameters, the homogenized problem can be made fully consistently with the reference heterogeneous problem. The consistency between the fine mesh heterogeneous problem and the homogenized problem was checked with a simple but highly heterogeneous problem. It was observed that the large errors such as about 1400 pcm in reactivity and 7 % in fission source distribution in the case without the angular discontinuity factors disappear with this approach.

An alternating calculation procedure involving the fine mesh S_N solution and the coarse S_N or S_2 solutions was established for the acceleration of the outer iterations in which the fast converging fission source distribution obtained is fed back into the fine mesh problem through the modulation scheme. The solution convergence of the accelerated case was examined first for the C5G7 benchmark problem. It was noted that the eigenvalue stabilizes very quickly around the converged value only after three heterogeneous S_N updates and the number of fine mesh S_N calculations could be reduced by a factor of roughly 50. In the examination of the core size dependency of the acceleration performance, the convergence of the coarse mesh S_N formulation did not reveal any noticeable performance degradation for larger problems. The number of fine mesh S_N updates stays around 7. The fact that the number of fine mesh heterogeneous S_N remains essentially unchanged with the core size is due to the ability of the coarse mesh S_N formulation which would lead to quick convergence of the global shape of the fundamental mode eigenfunction. Note that

the tight convergence of the coarse mesh problem renders sufficiently accurate global shapes of the fundamental eigenfunction while the partially converged fine mesh heterogeneous solution leads to the adjustment of local shapes of the fundamental eigenfunction. It was also confirmed that the S_2 coarse mesh formulation works as well. The speedup in terms of the computing time was measured for various problems and the maximum speedup of 84 was noted for the 9x9 quarter core problem.

With the above results, it can be concluded that significant acceleration of the S_N eigenvalue calculation can be achieved by using the angular flux discontinuity factors as well as angle dependent homogenized total cross sections in the homogenized coarse mesh S_N calculations while retaining the accuracy of the heterogeneous transport solution. Once the homogenized coarse mesh problem is constructed from a 2-D fine mesh heterogeneous solution, a global 3-D problem S_N can be formulated to incorporate the transport effect in the axial direction.

References

1. K. S. SMITH, “Assembly Homogenization Techniques for Light Water Reactor Analysis,” *Prog. Nucl. Energy*, **17**, p. 303-335 (1986).

2. H. G. JOO *et al.*, “Dynamic Implementation of the Equivalence Theory in the Heterogeneous Whole Core Transport Calculation,” *Proc. PHYSOR 2002,* Seoul, Korea, Oct. 7–10, 2002 (CD-ROM).

3. K. S. SMITH and J. D. RHODES, III, “Full-Core, 2-D, LWR Core Calculations with CASMO-4E,” PHYSOR2002, Seoul, Korea, Paper 13A-04, Oct. 7-10, 2002 (CD-ROM).

4. Y. JUNG *et al*., “Practical numerical reactor employing direct whole core neutron transport and subchannel thermal/hydraulic solvers,” *Ann. Nucl. Energy,* **62**, 357-374 (2013).

5. R. J.J. STAMMLER and M. J. ABBATE, *Methods of Steady-State Reactor Physics in Nuclear Design,* Chapter 6, Academic Press, London (1983).

6. A. YAMAMOTO, Y. KITAMURA and Y. YAMANE, “Cell homogenization methods for pin-by-pin core calculations tested in slab geometry,” *Annals of Nuclear Energy 31*, 825-847 (2004).

7. A. SEUBERT, “Pin Cell DFs in the Transient 3-D Discrete

Ordinates Code TORD-TD," *Proc. PHYSOR 2010*, Pittsburgh, Pennsylvania, USA, May 9–14, 2010 (CD-ROM).

8. A. Hebert, "A Consistent Technique for the Pin-by-Pin Homogenization of a Pressurized Water Reactor Assembly," *Nucl. Sci. Eng.*, **113**, pp. 227-238 (1993).

9. K. W. Park *et al.*, "Pin-Cell Homogenization via Generalized Equivalence Theory and Embedded Assembly Calculation," *Trans. Am. Nucl. Soc.*, **85**, 334-335 (2001)

10. Thomaz Kozlowski *et al.*, "Cell Homogenization Method for Pin-by-Pin Neutron Transport Calculations," *Nucl. Sci. Eng.*, **169**, 1-18 (2011).

초 록

본 연구에서는 비균질 세부 격자구조에 대한 수송계산의 효율적인 가속과 균질화된 소격격자 구조에 대한 수송계산의 기반을 확립하기 위하여 각불연속인자가 적용된 소격격자 모델을 구축하였고, 그 모델을 이용하여 이차원 비균질 세부 격자구조에 대한 수송계산을 가속하였다. 비균질 세부 격자구조에 대한 수송계산의 가속을 위하여, 먼저 부분적으로 수렴된 비균질 세부 격자구조의 수송계산 결과를 이용하여 균질화 인자를 생산하여 균질화된 소격격자 모델을 구축한 후, 균질화된 소격격자 모델에 대한 수송계산의 해를 이용하여 비균질 세부 격자구조에 대한 수송계산의 가속을 시행하였다. 비균질한 세부 격자구조와 동일한 균질화된 소격격자 모델을 구축하기 위하여 본 연구에서는, 새롭게 정의된 각불연속인자와 각도 의존 전단면적이 균질화된 소격격자 모델에 적용되었다. 각도 의존 전단면적이 부분적으로 수렴된 비균질 세부 격자구조의 수송계산 결과를 이용하여 바로 생산되는 데 반하여 각불연속인자

는 각불연속인자가 적용되지 않은 소격격자 모델에 대한 파일럿 연산의 해를 이용하여 얻어지게 된다. 이와 같은 공간 균질화에 더하여, 더 나은 가속 성능을 위해 각축약된 소격격자 모델을 제시하였다. 이렇게 구축한 균질화된 소격격자 모델의 해와 비균질 세부 격자구조의 해가 일치함을 확인하기 위하여, 여러 가지 일차원 및 이차원 비균질 문제에 대한 검증을 수행하였다. 각불연속인자와 각도 의존적 전단면적이 적용되지 않은 균질화된 소격격자 모델의 경우 비균질 세부 격자구조의 계산 결과와 비교하였을 때 반응도에 있어서 1400pcm, 핵분열 선원 분포에 있어서 7%의 오차가 나타났지만, 각불연속인자와 각도 의존적 전단면적이 적용된 균질화된 소격격자 모델의 경우 그러한 오차가 사라져 두 해가 완전히 일치함을 확인할 수 있었다.

이후 기 구축된 소격격자 모델을 이용하여 비균질 세부 격자구조에 대한 S_N 고유치 계산을 가속하여 수송계산의 계산 효율을 향상시키고자 하였다. 이러한 가속기법의 가속 성능을 확인하기 위하여 연료집합체 숫자가 각기 다른 다섯 종류의 노심

문제를 구성하였고, 가속기법이 적용된 경우와 가속이 적용되지 않은 경우의 계산 반복 횟수 및 계산 시간에 대한 비교를 수행하였다. 가속기법이 적용되지 않은 경우에는 문제의 크기에 따라 해를 도출하기 위한 반복 계산의 횟수가 계속해서 늘어나 비효율적인 계산이 이루어 졌지만, 가속기법이 적용된 경우 본래의 비균질 세부 격자구조의 계산 결과는 그대로 생산하면서 문제의 크기에 관계없이 10번 이내의 반복 계산만으로 해를 도출하는 것이 가능함을 확인 할 수 있었다. 즉, 소격격자 모델의 해의 수렴성이 문제의 크기에 관계가 없기 때문에 문제의 크기가 커질수록 가속기법의 효율성이 커지게 된다. 이를 검증하기 위하여 계산 시간에 있어서의 효율을 평가해 본 결과, 가속기법이 적용된 경우 가속기법이 적용되지 않은 경우에 비해 최대 84배 더 빠름을 확인하였고, 계산문제의 크기가 커질수록 가속성능도 더 커지는 결과를 얻을 수 있었다.

주요어:

각분할법
소격격자 모델
각불연속인자

학번: 2012-23284